

IITRI Project A6122
(Final Report)

AN AIRBORNE EXPERIMENT TO DETERMINE
TEMPERATURE VARIATIONS THROUGHOUT
THE SOLAR CORONA DURING THE
ECLIPSE OF 12 NOVEMBER 1966

National Aeronautics & Space Administration
Office of Research Grants & Contracts
Washington, D.C. 20546

IITRI ~~Project~~ A6122
(Final Report)

AN AIRBORNE EXPERIMENT TO DETERMINE
TEMPERATURE VARIATIONS THROUGHOUT
THE SOLAR CORONA DURING THE
ECLIPSE OF 12 NOVEMBER 1966

Contract No. NASr-65(12)

Prepared by

G. Henderson

IIT Research Institute
Technology Center
Chicago, Illinois 60616

Submitted to

National Aeronautics and Space Administration
Office of Research Grants & Contracts, Code BG
Washington, D.C. 20546

Attention: Technical Reports Officer

March 1967

IIT RESEARCH INSTITUTE

*1100
change
to
contract.*

FOREWORD

This is the Final Report to NASA on Contract NASr-65(12), IITRI Project No, A6122, entitled, "An Airborne Experiment to Determine Temperature Variations Throughout the Solar Corona During the Eclipse of 12 November 1966." This report is preliminary in that it is being issued prior to reduction of the data and is intended to describe the experiment and instrumentation, Subsequent reports will cover results obtained.

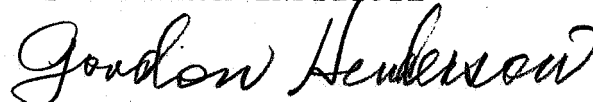
The period of the contract extended from 1 April 1966 until 31 January 1967. The work involved the design, construction and installation of an optical system to measure coronal temperatures during the 12 November 1966 eclipse of the sun, The system was installed on board the NASA Convair 990, "Galileo," along with other experiments to be performed during the eclipse. The observation was essentially a repetition of ground level measurements taken during the 1965 eclipse in the Cook Islands which was unsuccessful due to cloud cover during totality. The use of an aircraft on this occasion practically ensured good seeing conditions and also prolonged totality by 75%.

Some 45 line-profile measurements of the $\lambda 5303\text{\AA}^{\circ}$, Fe XIV emission were obtained during the eclipse from which a similar number of temperature measurements will be obtained after analysis.

III RESEARCH INSTITUTE

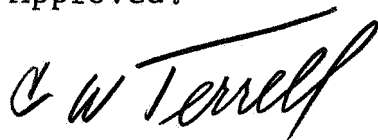
The maximum displacement from the sun's limb at which ,results were obtained was $0.8 R_o$, where R_o represents the solar radius. Previously, the maximum displacement at which results were obtained at a similar phase of the solar cycle was $0.3 R_o$. This observation , therefore, represents an increase of almost a factor of 3 in the extent of this type of measurement and indicates that the interferometer system employed has a significant role to play in coronal studies. Detailed analysis of all data obtained is expected to be performed under a subsequent program and will require approximately 6 months to complete.

Respectfully submitted,
IIT RESEARCH INSTITUTE



Gordon Henderson
Research Physicist
Optics Research

Approved:



C. W. Terrell
Director
Physics Research

IIT RESEARCH INSTITUTE

ABSTRACT

The IITRI Scanning Fabry-Perot interferometer, named PRISM (Photoelectrically Recording Interferometer Scanned Magnetostrictively), was incorporated into an optical system installed on board the NASA Convair 990, "Galileo", for observation of the 12 November 1966 eclipse of the sun. During the eclipse the aircraft followed the moon's shadow at an altitude of about 40,000 feet resulting in a totality period of 206 seconds compared to a corresponding ground totality of about 115 seconds. Some 45 line profiles of the $\lambda 5303\overset{\circ}{\text{A}}$, Fe XIV emission were obtained from which a similar number of Doppler temperatures will be obtained after analysis. The maximum displacement from the solar limb at which measurements were obtained was 0.8 solar radii representing an improvement of almost a factor of 3 over the best previous results at a similar phase of the solar cycle.

TABLE OF CONTENTS

	<u>Page</u>
FOREWORD	ii
ABSTRACT	iv
I. INTRODUCTION	1
II. DISCUSSION OF TOTAL EXPERIMENT	3
A. Eclipse Parameters	3
B. Equipment	5
C. Instrumentation	12
D. Aircraft Installation	12
E. Equipment Alignment and Simulation Flights	16
F. Eclipse Flight	28
III. RESULTS AND ANALYSIS	29
IV. CONCLUSIONS AND SUGGESTIONS FOR FURTHER WORK	34
ACKNOWLEDGEMENTS	
REFERENCES	
APPENDIX A - A New Design of a Scanning Fabry-Perot Interferometer	
APPENDIX B - Halfwidth Error Analysis	

TABLE OF CONTENTS (continued)

FIGURE LIST

<u>Figure No.</u>		<u>Page</u>
1	Path of Ground Totality for the Eclipse of November 12, 1966	4
2	Showing the General Layout of the Optical System for the Aircraft Installation to Investigate Coronal Emission Profiles	6
3	Variable-Deviation Wedge, 00' - Optical Axis	7
4	Deviating Wedge Assembly	8
5	Showing Layout of Two Fabry-Perot Interferometers to Record $\lambda 5303A$ and $\lambda 6374A$ Emission Profiles	10
6	Beam Splitter and Interferometer Assembly	13
7	Complete Optical Assembly	14
8	Floor Plan of NASA Convair 990 "Galileo" for Eclipse Expedition, November, 1966	15
9	Installation Assembly in CV 990	17
10	Frame Installation	18
11	Wedge Drive Assembly	19
12	Collimator Assembly	20
13	Interferometer Mount	21
14	Photomultiplier Assembly	22
15	Frame for Electronics Installations	23
16	Showing Optical System (Left side of Aircraft)	24
17	Showing Electronic Amplifying and Recording System (Right Side of Aircraft)	25

TABLE OF CONTENTS (continued)

FIGURE LIST (continued)

<u>Figure No.</u>		<u>Page</u>
18	Showing the Profiles of the Hg $\lambda 5461\text{\AA}$ Emission as Measured by the $\lambda 5303\text{\AA}$ Interferometer Immediately after the Eclipse	27
19	Showing Raw Data Obtained at a Scanning Rate of 2 Scans per Second	30
20	Showing Raw Data for a Scanning Rate of about 3 Seconds per Free Spectral Range (3.2A)	31

AN AIRBORNE EXPERIMENT TO DETERMINE
TEMPERATURE VARIATIONS THROUGHOUT
THE SOLAR CORONA DURING THE
ECLIPSE OF 12 NOVEMBER 1966

I. INTRODUCTION

The solar corona presents several outstanding problems in the field of solar physics. Chief among these remains the question of the source of coronal heating, and the various theories which are currently undergoing examination require observational information on the coronal temperature, density, and magnetic field patterns. Several observatories throughout the world are engaged in regular studies of the corona through the use of the coronagraph; however, the extent of observations beyond the solar limits is greatly restricted by the scattering of sunlight by the instrument and the earth's atmosphere. Development of satellite-borne coronagraphs is now at an advanced stage but it is reasonable to assume that, at least for the duration of the next solar cycle, observers will mainly depend upon ground-based instruments. The other situation which permits investigation of the corona is during a total eclipse of the sun. On these occasions ordinary astronomical instruments can be used to observe the corona, and observations can be made to a much greater distance out from the solar limb. .

Until recently, coronal temperatures showed a variation between $0.8 \times 10^6 \text{K}$ (Allen¹) and $2.5 \times 10^6 \text{K}$ (Dollfus², Billings³, Jarrett and von Klüber⁴). The lower temperatures were obtained by ionization data and radio brightness measurements; the higher temperatures were obtained by line profile determinations interpreted on the basis of a homogeneous corona in hydrostatic equilibrium. In the last two years further theoretical work has helped to resolve the disagreement between some of the methods (Burgess⁵, Brandt, Michie and Cassinelli⁶), and a coronal temperature in the region of $2 \times 10^6 \text{K}$ is obtained from all of the methods with the exception of the radio brightness method. The value of $2 \times 10^6 \text{K}$ refers to the average undisturbed corona and does not preclude the existence of higher temperatures in specific regions such as in the neighborhood of active regions in the photosphere.

The purpose of the observation to be described here was to obtain a series of temperature measurements at various points in the corona by the method of emission line profile determinations. The instrument used to obtain the profiles was a scanning type of Fabry-Perot interferometer which is fully described in Appendix A of this report. Early attempts to obtain interference fringes of the coronal lines using Fabry-Perot interferometers⁷ were unsuccessful for various reasons up until the eclipse of 1954 when Jarrett and von Klüber⁸ succeeded in obtaining photographs of the $\lambda 5303 \text{\AA}$, Fe XIV emission. At the eclipse of 1958 these authors succeeded in

obtaining several good photographs of the Fe XIV and also the Fe X ($\lambda 6374\overset{o}{\text{\AA}}$) emissions⁴. During the eclipse of 30 May 1965, the author attempted to measure the $\lambda 5303\overset{o}{\text{\AA}}$ emission line using the scanning Fabry-Perot interferometer and photoelectric detection. Unfortunately, cloud cover during totality prevented any results from being obtained,

II. DISCUSSION OF TOTAL EXPERIMENT

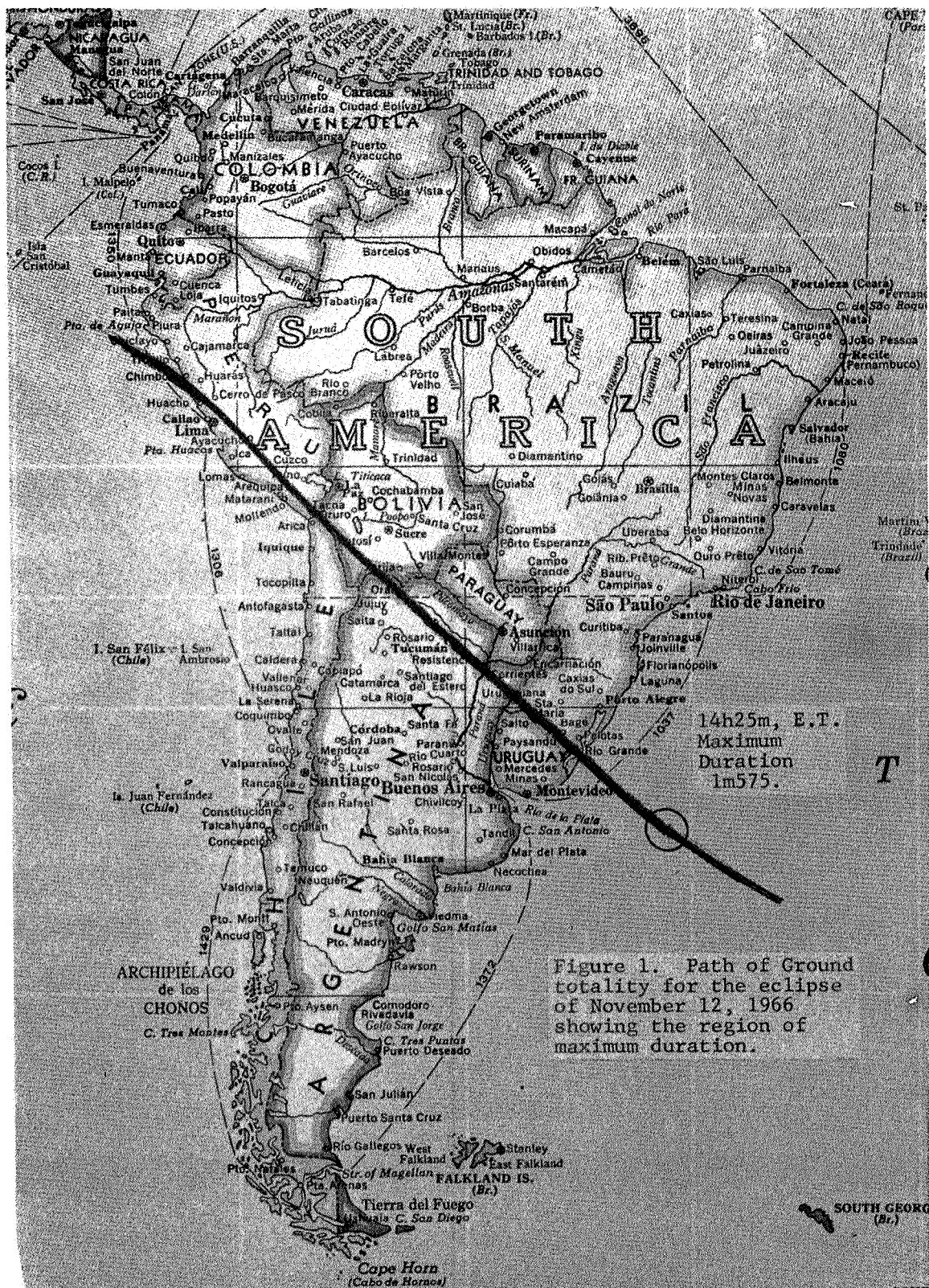
A. Eclipse Parameters

Figure 1 shows the path of ground totality over the South American continent for the eclipse of 12 November 1966. Marked on the path is the location of maximum duration of totality, some 500 miles east of the entrance of the River Plate. The parameters of the eclipse at this location were:

Ephemeris Time	1425 hours
Local Mean Time	1121 hours
Sun's Altitude	70°
Shadow Speed	1332 knots
Duration of Maximum Totality	117 seconds

The instrumentation was installed on board the **NASA** Convair 990, "Galileo", along with that of other observers. During the period of the eclipse expedition, the aircraft was based at Porto Alegre in Southern Brazil and, on eclipse day, intercepted the shadow approximately 100 miles northwest of the

IIT RESEARCH INSTITUTE



point of maximum totality at an altitude of 40,000 feet. Flying a course in the same general direction as that of the shadow, the duration of totality was extended to 206 seconds.

B. Equipment

The general layout of the optical system is shown in Figure 2. Light from the corona is directed to the objective via the variable wedge and folding mirror. The objective focuses the field onto the aperture whose size governs the angle of acceptance of the telescope. In operation, the system is initially aligned on the sun's center with the variable wedge aligned to have zero effect on the incoming light, Figure 3 shows the principle of operation of the wedge assembly. The two composite wedges can have any orientation relative to each other, the resultant effect upon a light beam being similar to that of a single wedge at a specific orientation. Hence, for a fixed relative orientation of the component wedges, the field of view is deflected by a specific amount, and rotation of the complete assembly about the optic axis provides a circular sweep of the field, Figure 4 shows a photograph of the wedge assembly with its associated drive system. After the initial alignment, the gyro-stabilized heliostat is locked in and a relative rotation of the wedge assembly to the first position brings the region of the corona at $1.1 R_o$, where R_o is one solar radius, onto the aperture. The position angle with

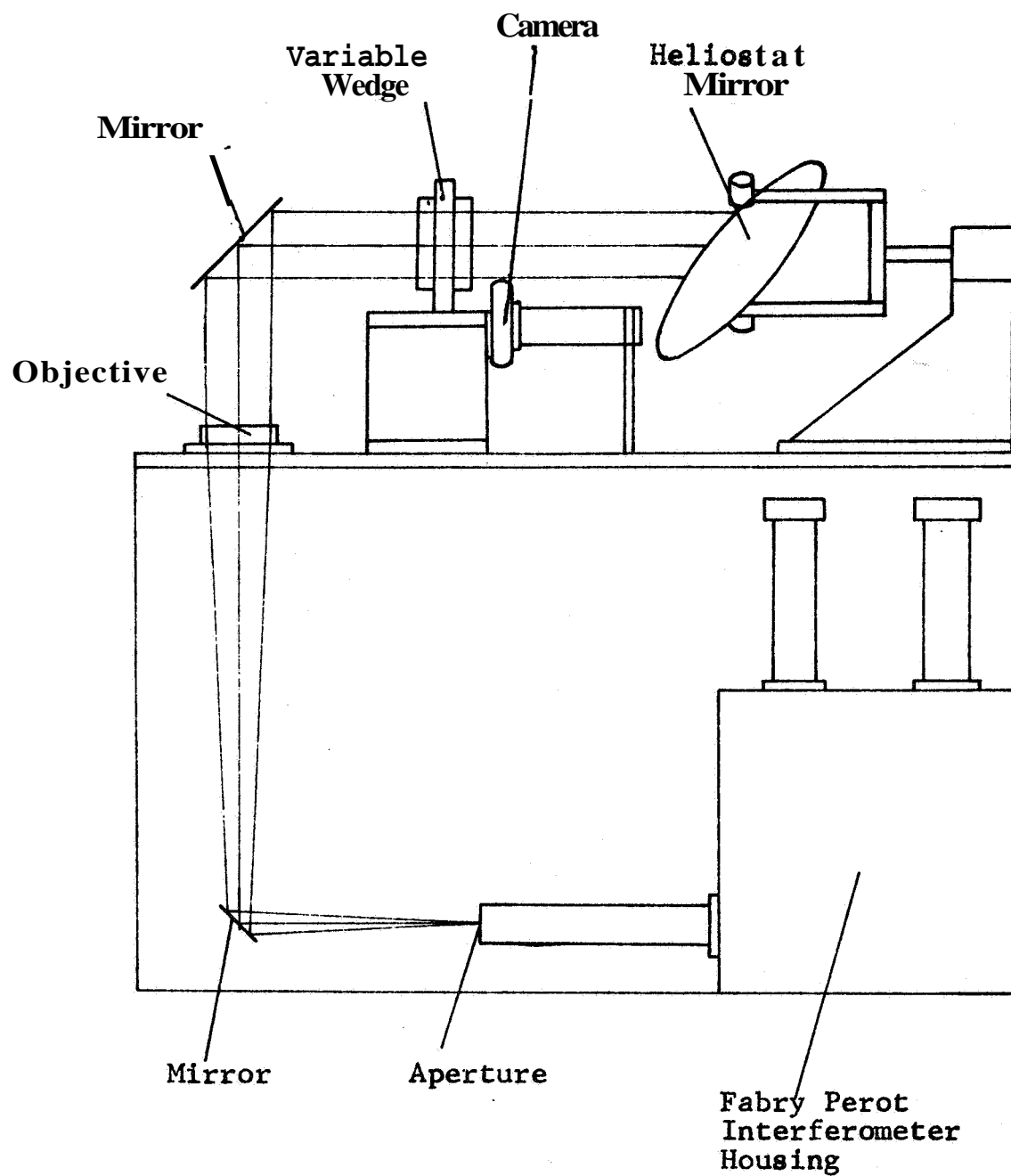


Fig. 2 Showing the General Layout of the Optical System for the Aircraft Installation to Investigate Coronal Emission Profiles.

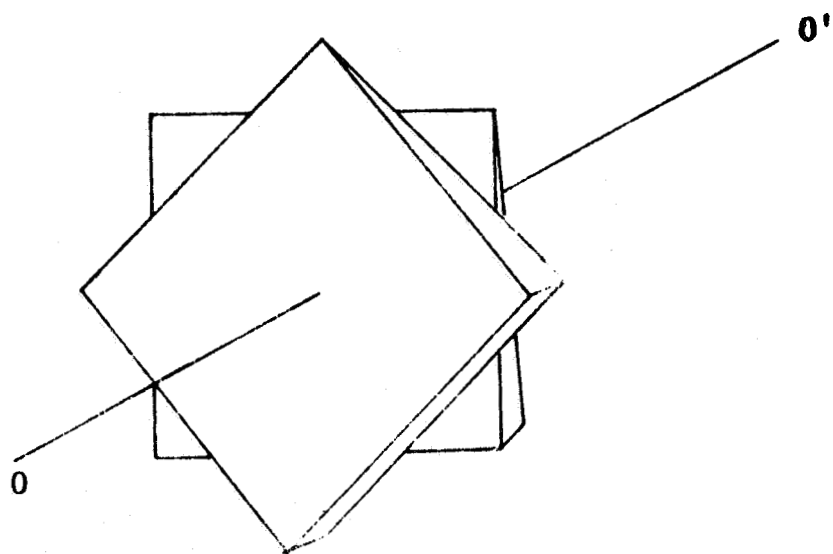


Figure 3. Variable-Deviation Wedge
00' - Optical Axis

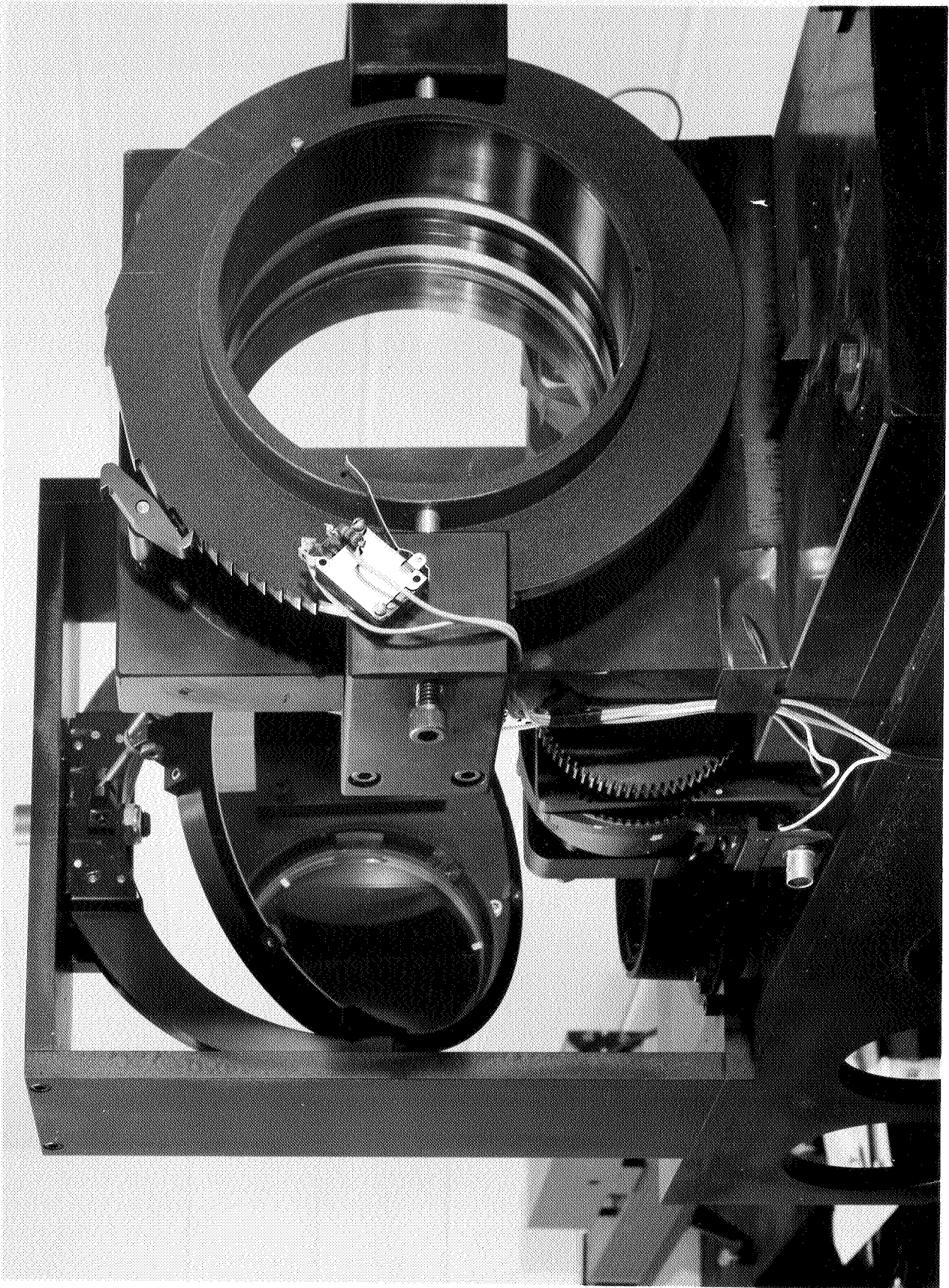


Fig. 4 Deviating Wedge Assembly

u

respect to the sun which is initially viewed depends upon the circumstances of the observation and can easily be calculated. During the eclipse, the drive system of the wedge assembly provides a rotation of the field at the selected radial distance from the sun's center. After each rotation, an automatic change in radius is made and the rotation is repeated. This operation takes place continuously during the eclipse, and a continuous recording of the instantaneous field of view is made.

Figure 5 shows the optical arrangement after the light has passed through the aperture. Coronal light transmitted by the aperture is collimated at the entrance to the interferometer housing. **Two** scanning Fabry-Perot interferometers are installed to provide a redundant system. The design is such that the back-up Fabry-Perot is used to provide scans of the $\lambda 6374\overset{o}{\text{\AA}}$ Fe X emission line while the main interferometer is scanning the $\lambda 5303\overset{o}{\text{\AA}}$, Fe XIV, emission. Both emissions are obtained from the same field of view defined by the field aperture. Should the $\lambda 5303\overset{a}{\text{\AA}}$ Fabry-Perot, or its associated circuitry, fail during the observations, the system is designed to change to the back-up instrument in about 10 seconds. After collimation the light entering the interferometer box falls on the dichroic beamsplitter, and the red region of the spectrum containing the $\lambda 6374\overset{o}{\text{\AA}}$ line is reflected through 90° . The two emission lines are isolated by the narrow band filters before traversing their respective interferometers. Finally,

IIT RESEARCH INSTITUTE

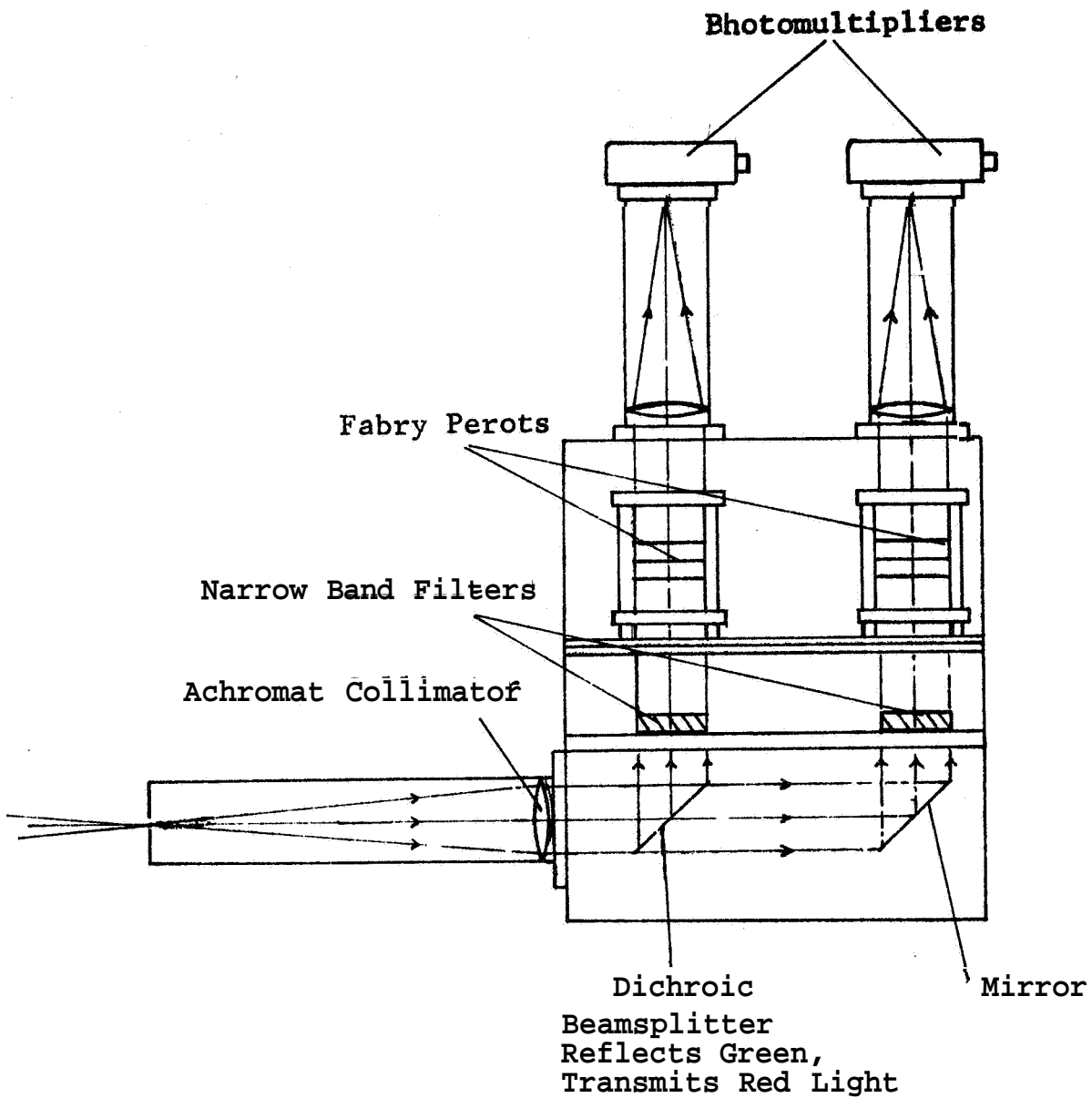


Fig. 5 Showing Layout of Two Fabry Perot Interferometers to Record $\lambda 5303A$ and $\lambda 6374A$ Emission Profiles

the transmitted light from the two Fabry-Perots falls on two separate and independent detection systems consisting of identical photomultipliers whose outputs are simultaneously displayed on an oscilloscope and recorded on a high speed strip chart recorder, Continuous visual monitoring of the outputs of both interferometers during operation is provided by the oscilloscope and, hence, a failure of either interferometer system is immediately apparent, Should the $\lambda 5303\overset{\circ}{\text{\AA}}$ fail, a rapid change-over to the back-up interferometer is effected by removal of the dichroic beamsplitter from the light beam and replacement of the $\lambda 6374\overset{\circ}{\text{\AA}}$ narrow band filter by the $\lambda 5303\overset{\circ}{\text{\AA}}$ filter. The dual system does not cause any light loss compared to a single interferometer arrangement because the dichroic beamsplitter is a non-absorbing device and, hence, either transmits or reflects all incident light.

By employing the back-up system to provide line profiles of the $\lambda 6374\overset{\circ}{\text{\AA}}$ emission, a much greater scientific value is attached to the observations, The temperature distribution in the corona can now be obtained from:

- (1) Line profiles of $\lambda 5303\overset{\circ}{\text{\AA}}$, Fe XIV, and $\lambda 6374\overset{\circ}{\text{\AA}}$, Fe X emissions, each of which will provide a value for the Doppler temperature.
- (2) The intensity ratio of the Fe XIV and Fe X emissions; a value for the temperature can be obtained from ionization theory, assuming ionization equilibrium to exist throughout the corona.

IIT RESEARCH INSTITUTE

Figure 6 is a photograph of the box containing the beamsplitter and Fabry-Perot interferometers, and Figure 7 is a photograph of the complete optical assembly without the heliostat,

C. Instrumentation

The detection and recording system for each interferometer consists of a cooled RCA 1P21 photomultiplier, a Keithley picoammeter, and a mirror-galvanometer recorder. The over-all response time of the system is about 10 milliseconds. Each interferometer output is recorded on two channels of the recorder, the ratio of the full scale deflections being 2:1. This feature provides a back-up for each emission line in the recording system. Other channels in the recorder are devoted to the instantaneous current through each interferometer and the position in the corona being observed. The positional information is represented by the angular distance and position angle with respect to the sun's center.

D. Aircraft Installation

Figure 8 shows the floor plan of "Galileo", used for the eclipse expedition. The observation windows, which were specially installed for the 1965 eclipse, were arranged along the left side of the aircraft at an elevation of 65° . The elevation of the sun at second contact in the 1966 eclipse

MIT RESEARCH INSTITUTE



Fig. 6 Beam Splitter and Interferometer Assembly

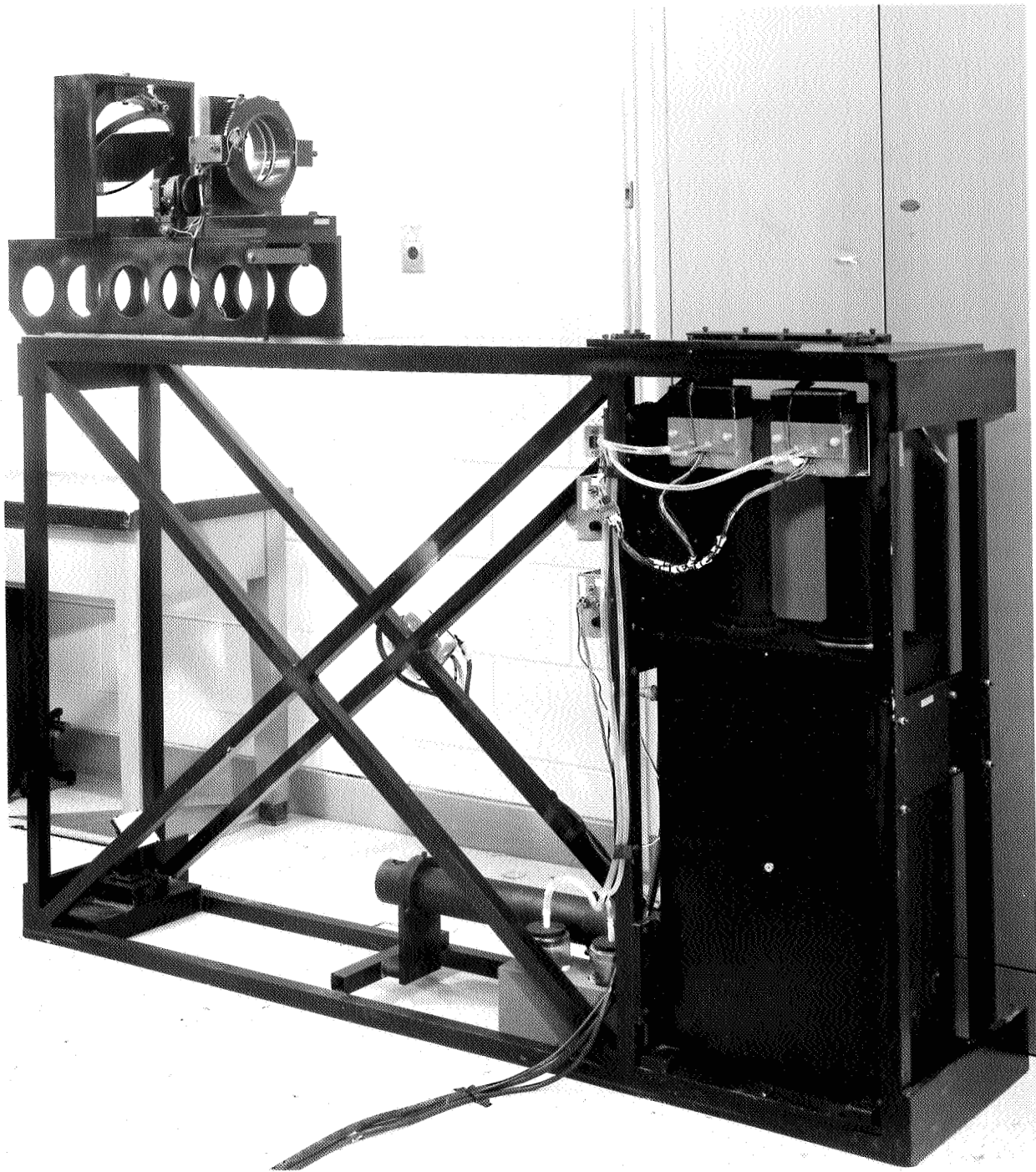


Fig. 7 Complete Optical Assembly

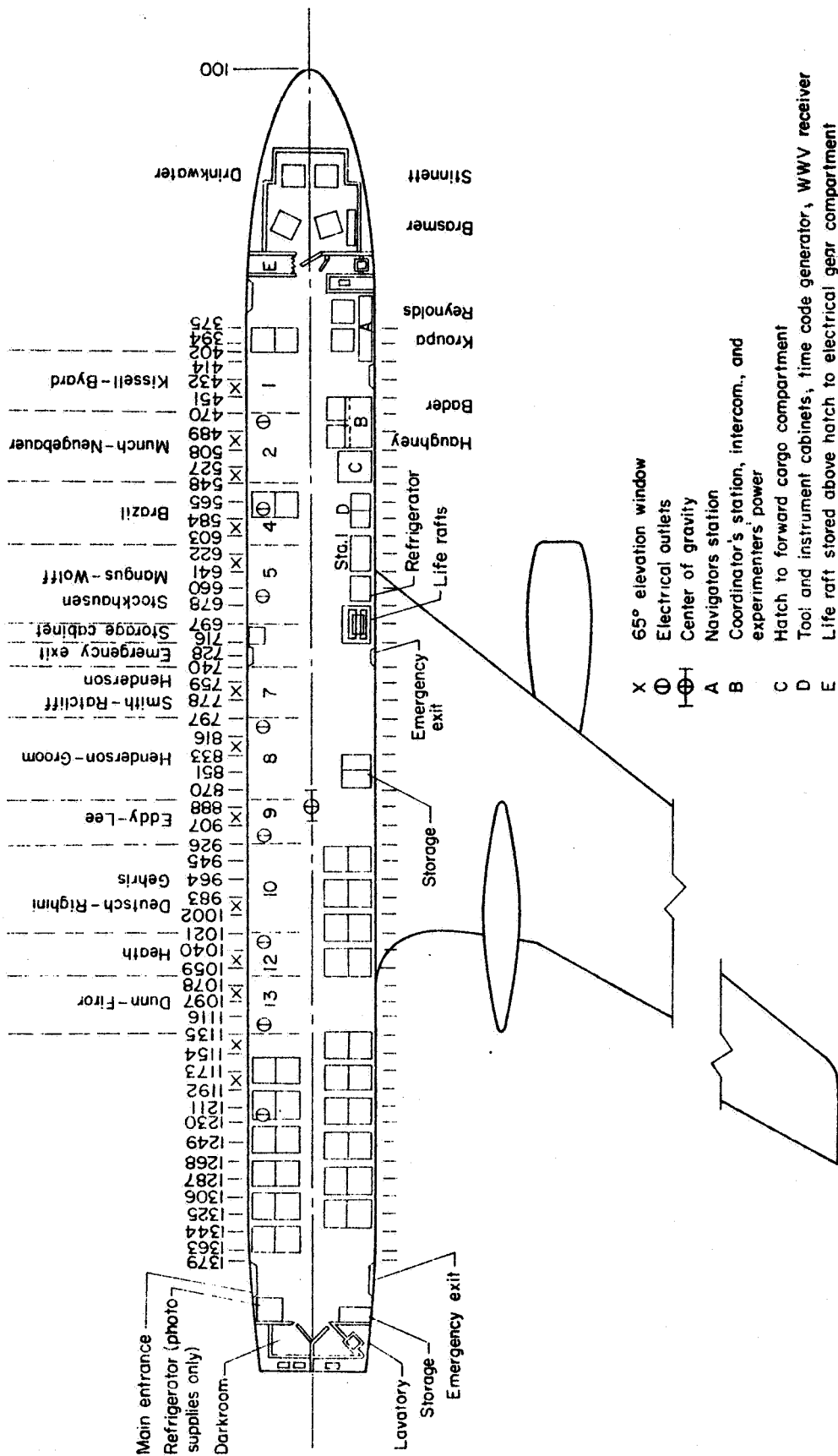


Fig. 8 Floor Plan of NASA Convair 980 "Galileo" for Eclipse Expedition, November, 1966

was expected to be near 70° but no problems were expected from the slight departure from normal incidence. This prediction was verified during the practice flights. Figures 9 to 15 and Figure 6 show the assembly drawings for the complete aircraft installation and Figures 16 and 17 are photographs of the equipment on board the aircraft.

The installation of the equipment was started on 26 September 1966, and was completed, along with the installations of other experiments, on 18 October 1966. The installation was carried out at Ames Research Center, Moffett Field, California, with the technical assistance of NASA/Ames personnel.

E. Equipment Alignment and Simulation Flights

Initial alignment of the equipment was carried out while the aircraft was on the ground. The alignment consisted of bringing the optical axis of the telescope system into line with the fore-and-aft axis of rotation of the heliostat. The whole assembly was autocollimated using the heliostat mirror. Finally, a resolution check on the interferometers was obtained using a Hg $\lambda 5461\overset{o}{\text{\AA}}$ source.

For the flight tests, the autocollimation procedure was undergone after each take-off, followed by a resolution check with the Hg source. The equipment was in no way shock mounted and it was observed that there was a noise contribution

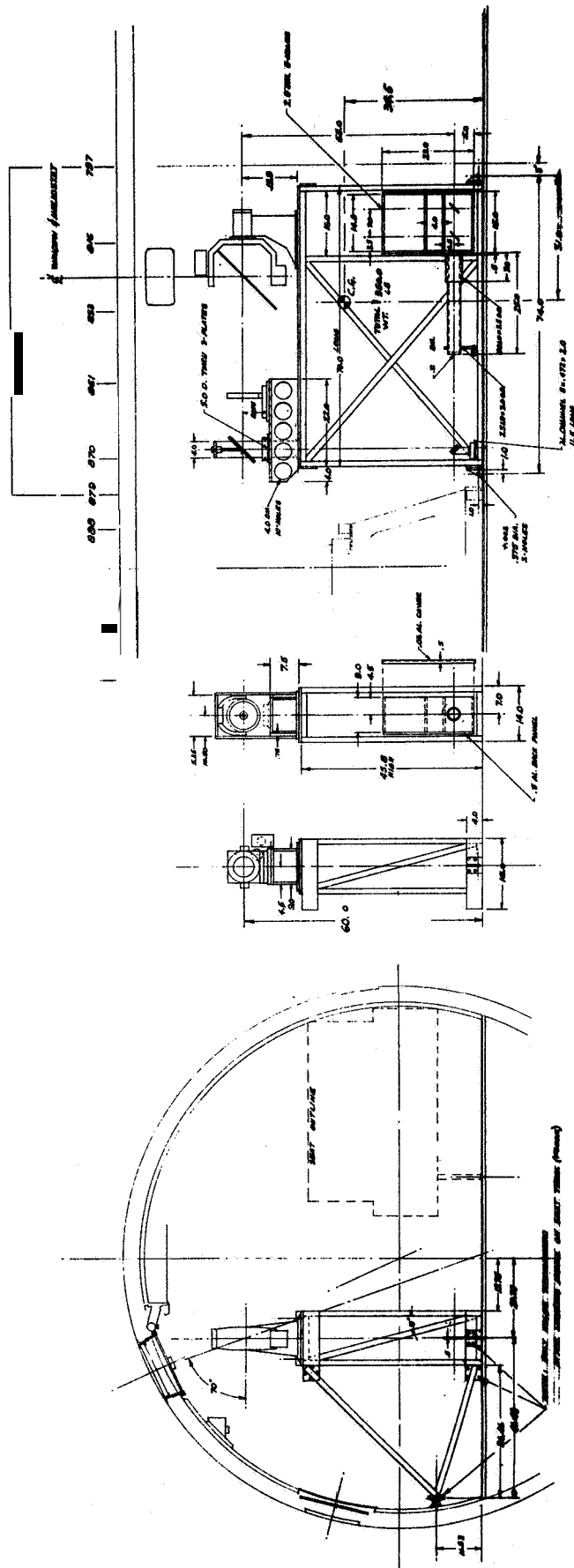
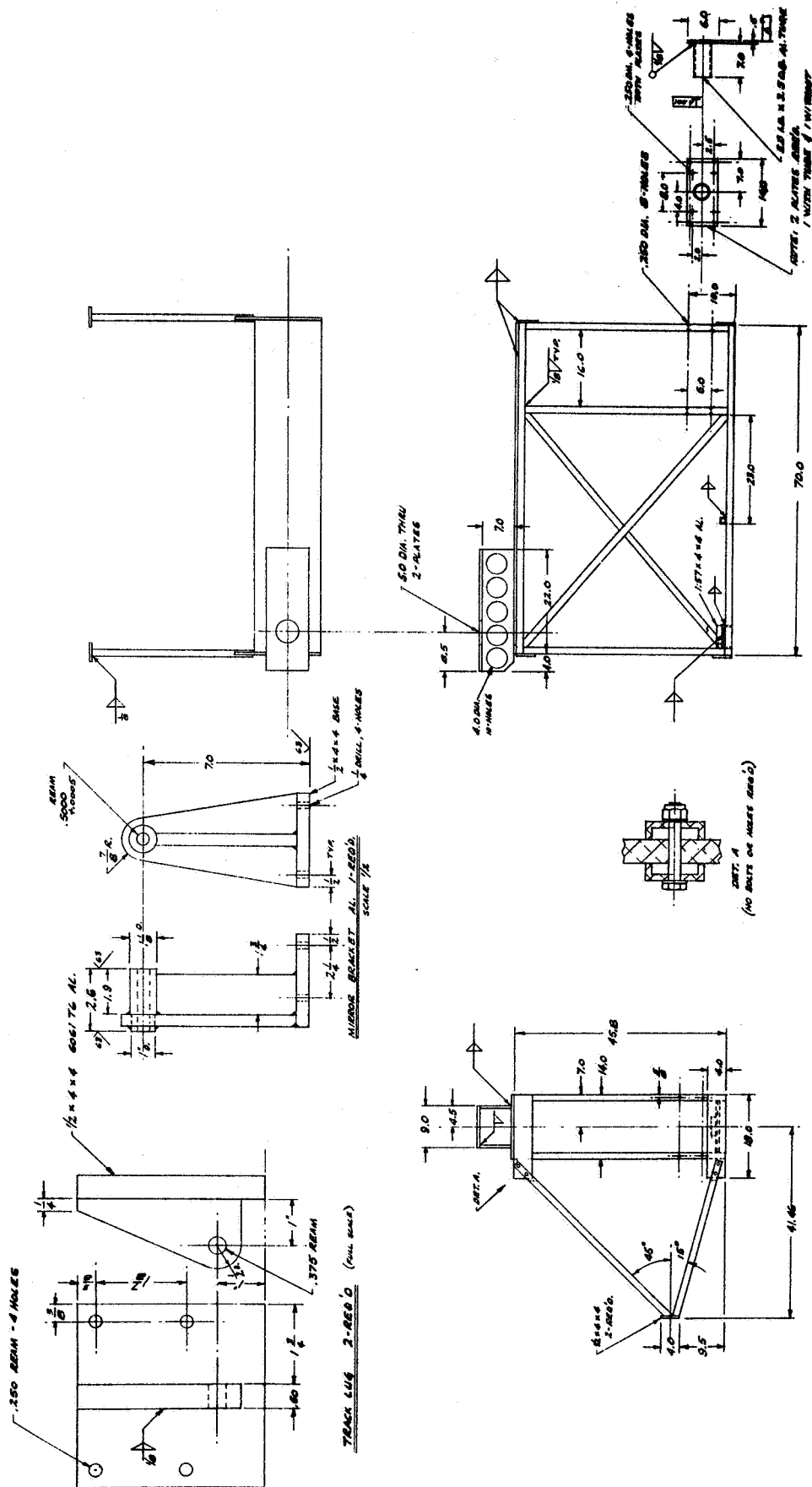


Fig. 9 Installation Assembly in 990



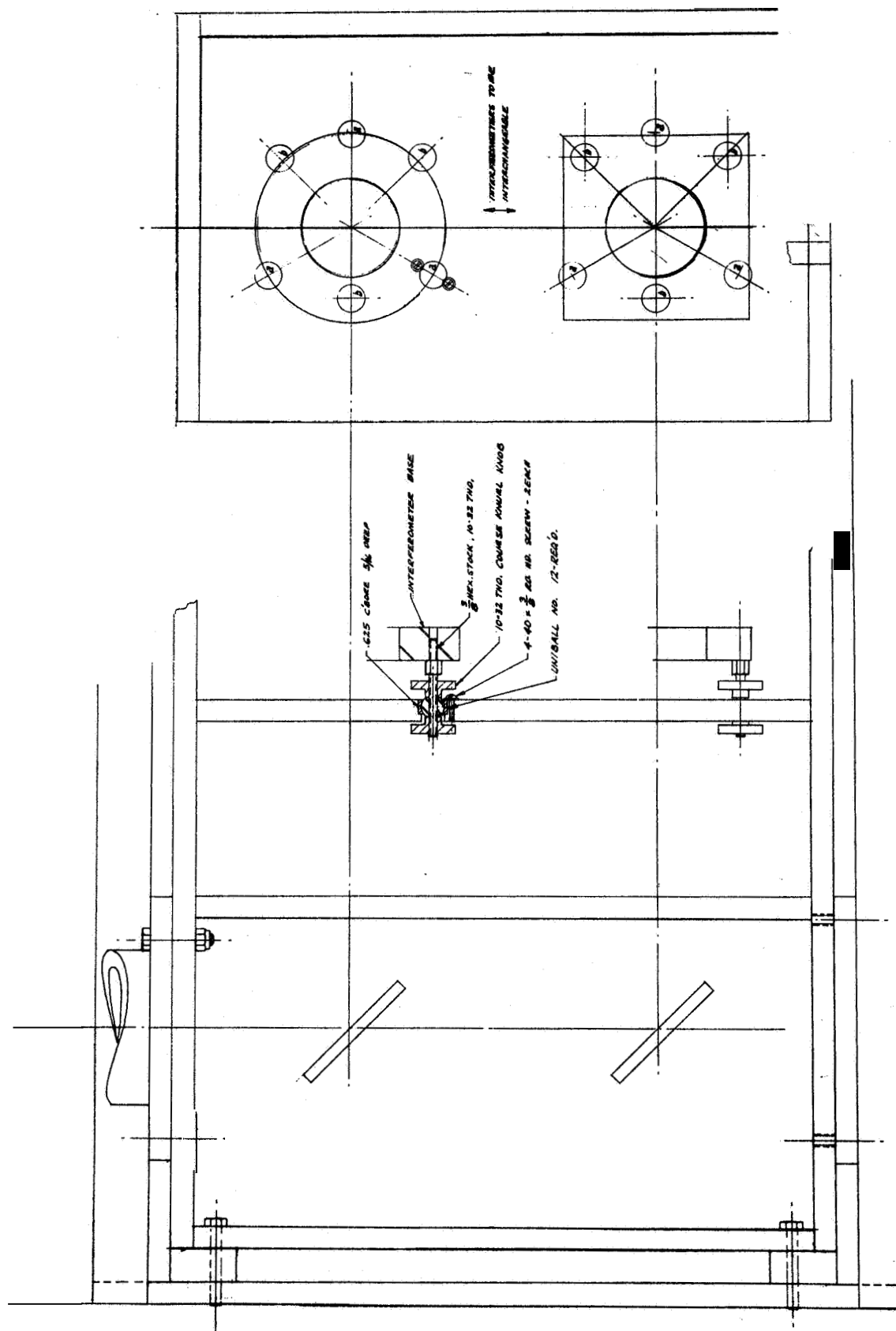


Fig. 13 Interferometer Mount

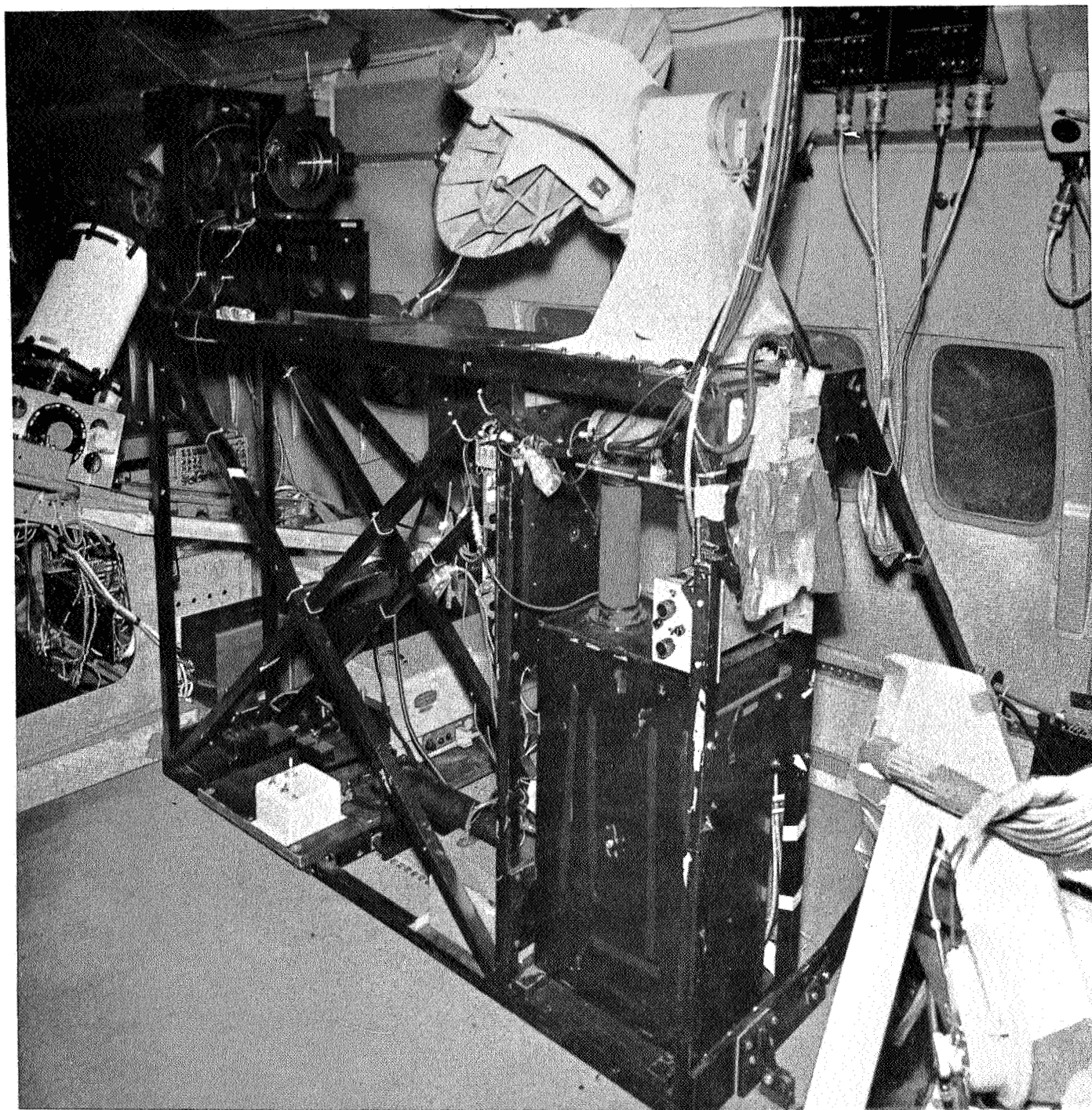


Fig. 16 Showing Optical System (Left side of Aircraft)

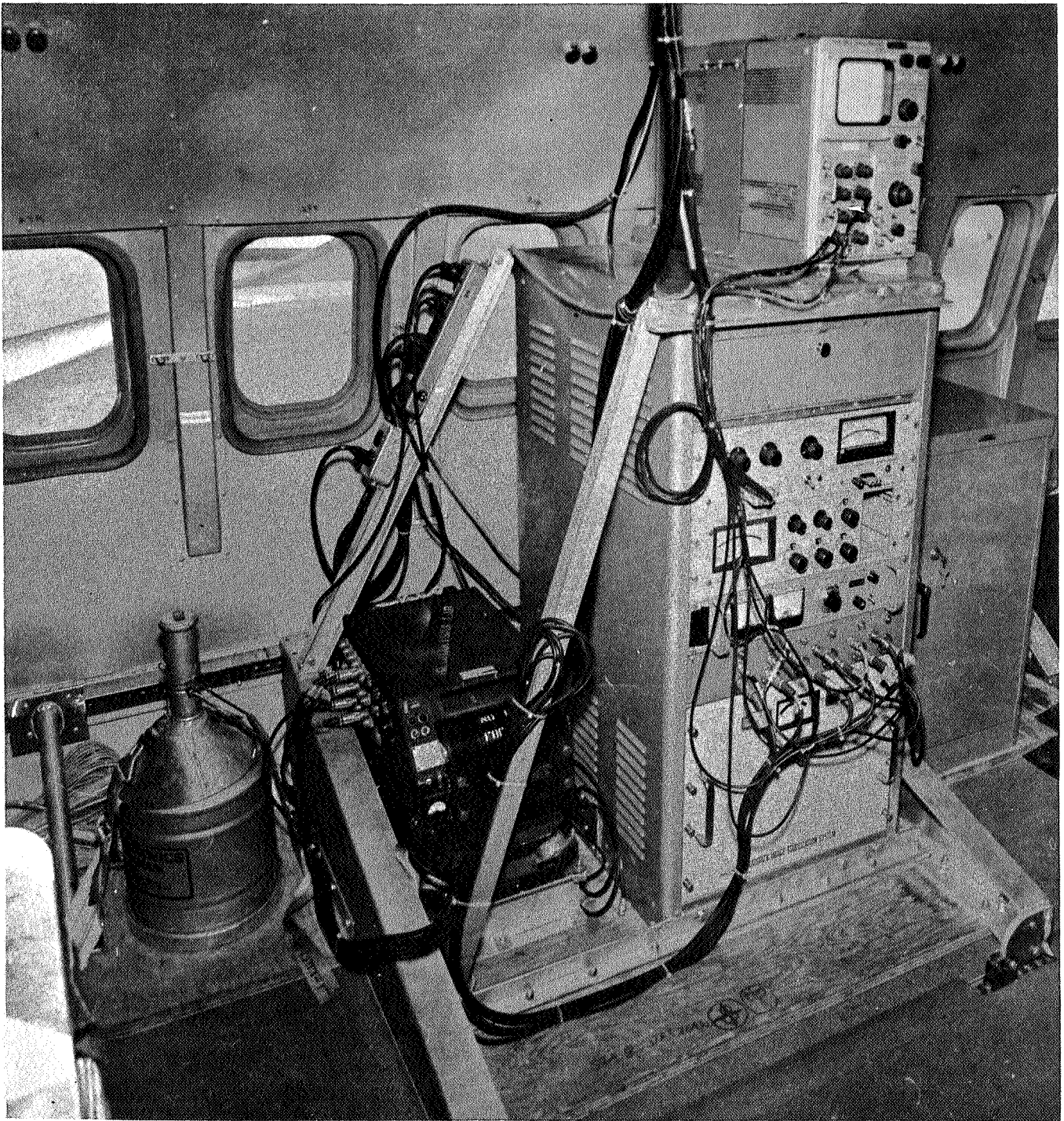


Fig. 17 Showing Electronic Amplifying and Recording System (Right Side of Aircraft)

to the signal at a frequency of about 200 cps. This did not prevent the satisfactory operation of the system as the fastest scanning rate was a factor of 100 times less than the frequency of the vibration. Figure 18 shows an example of the line profiles obtained in flight on the $\lambda 5461\overset{o}{\text{\AA}}$ emission.

For the purposes of eclipse simulation during the practice flights, the aircraft was flown to a latitude which permitted the sun, or on night flights, the moon, to be observed at, or near, the eclipse altitude of 70° . A curved path, which maintained the relative bearing of the sun constant, was flown for a period of about 15 minutes. The in-flight drift rate of the gyro-stabilized heliostat was checked during this time and a 5 minute totality simulation was counted off during which time observers carried out their eclipse drills. In all, two day and two night flights were carried out from Moffett Field.

On Wednesday, 2 November 1966, Galileo, with about 40 experimenters, crew and support personnel on board, departed Moffett Field for Porto Alegre, Brazil. The expedition arrived at Porto Alegre on 3 November 1966 after an overnight stop at San Juan, Puerto Rico. During the interval until eclipse day, 12 November 1966, three more navigation and practice flights were carried out,,

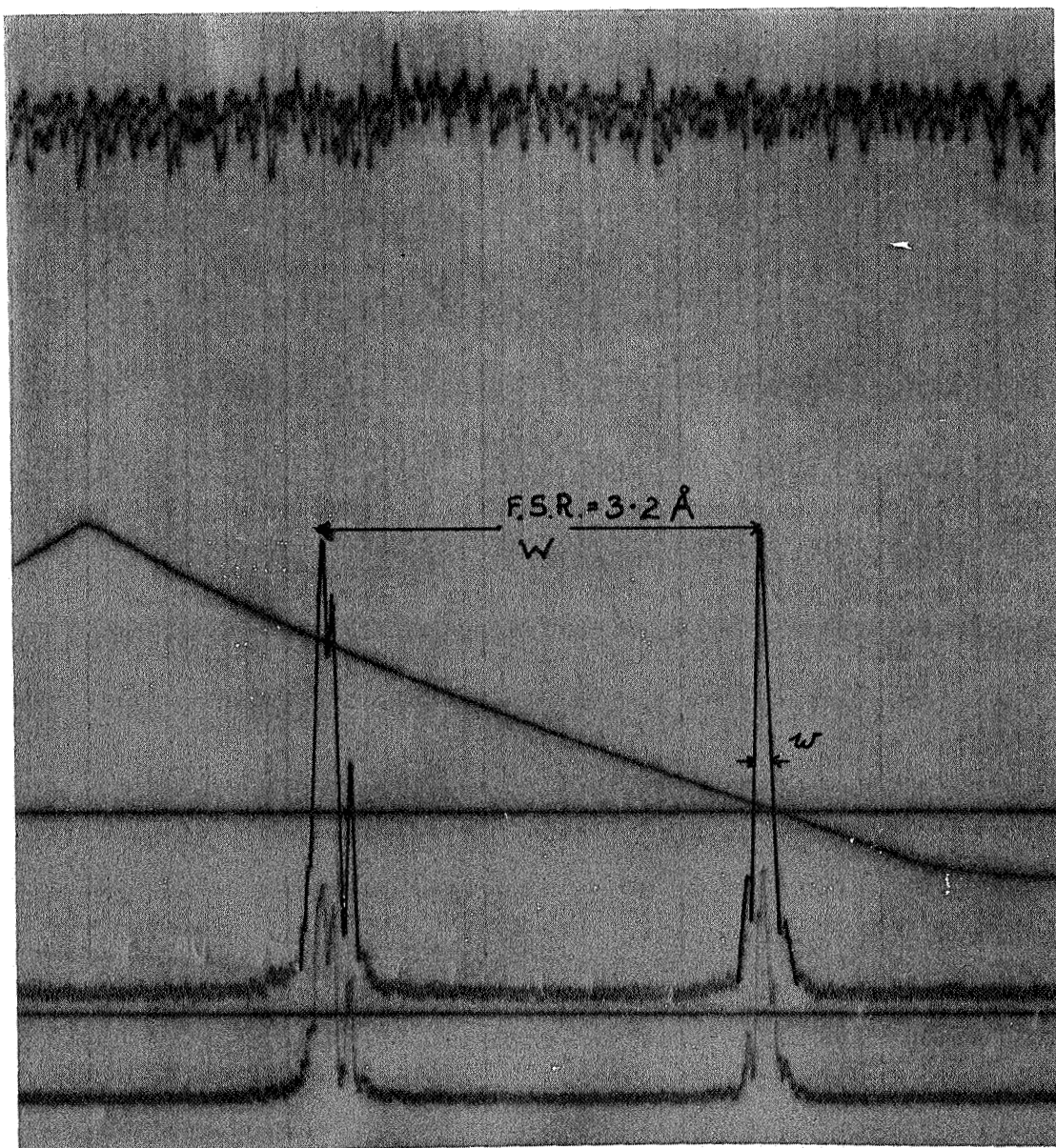


Figure 18 Showing the profiles of the $\text{Hg } \lambda 5461\text{\AA}$ emission as measured by the $\lambda 5303\text{\AA}$ interferometer immediately after the eclipse. The different apparent widths in the **two** orders is due to the non-linearity of the magnetostrictive effect. This effect is allowed for in obtaining the true line profile. The effect of noise is more apparent when observing such a narrow line compared to the coronal emission but a reasonable value for the instrumental function can still be obtained, viz:-

$$\Delta h = \frac{\omega}{W} \times \text{FSR} = \frac{1}{24} \times 3.2 = 0.13\text{\AA}$$

Part of the trace has been overwritten to compensate for the poor reproduction quality of the data paper.

F. Eclipse Flight

On the eclipse flight, Galileo intercepted the umbra at 14 hours, 16 seconds, 57 seconds, U.T., at a position $34^{\circ} 26'$ South, $49^{\circ} 51'$ West. Totality lasted for 206 seconds. During totality, line profiles of the $5303\overset{\circ}{\text{\AA}}$, Fe XIV emission were recorded. The back-up interferometer, which was arranged to measure the $\lambda 6374\overset{\circ}{\text{\AA}}$, Fe X emission, developed a malfunction shortly before totality and no traces of the $\lambda 6374\overset{\circ}{\text{\AA}}$ line were obtained. The signal from the interferometers was continuously observed on the oscilloscope screen and amplifier gains were adjusted, when required, to maintain the signal within pre-determined limits.

The designed spectral scanning rate of the interferometers was one scan per half second. It was expected that the higher noise present with such a fast scan rate would cause a loss of signal at some time before the end of totality and it was arranged in the eclipse drill to change to a slow manual scan with the inclusion of electronic damping to reduce the noise when the signal-to-noise ratio on the fast scan rate fell to about 2:1. During the eclipse, emission line profiles were obtained out to 1.5 solar radii with the scan rate of 2 scans per second. The manual scanning procedure was then introduced at a rate of about one scan per 3 or 4 seconds, and line profiles were obtained out to 1.8 solar radii from the sun's center when third contact stopped further observations.

During the slow scans the look direction in the corona was maintained close to Position Angle 90° for the different displacements from the sun's center.

III. RESULTS AND ANALYSIS

Figure 19 shows an example of the raw data obtained with the scanning rate of 2 scans per second. Figure 20 shows an example of the raw data obtained at a scanning rate of one scan per 3 seconds.

The observed profiles are effectively the convolution of the true profile of the emission, the instrumental function of the Fabry-Perot interferometer and the transmission function of the narrow-band forefilter.

To obtain the true emission profile, first, a proper curve must be drawn through the rough data curve to eliminate the noise contribution. Next, by using the instrumental function derived from the $\text{Hg } \lambda 5461\text{\AA}$ profiles as shown in Figure 18, the true instrumental profile is obtained. The Doppler half-width of the $\lambda 5461\text{\AA}$ emission line from the uncooled Hg source is 0.006\AA . The instrumental function of the Fabry-Perot interferometer was calculated from the measured reflectance and spacing of the plates to be 0.13\AA . Therefore, the observed profiles shown in Figure 18 are essentially due to the instrumental function of the interferometer only. The transmission function of the narrow band forefilter is now convoluted with the known Fabry-Perot instrumental function to provide an

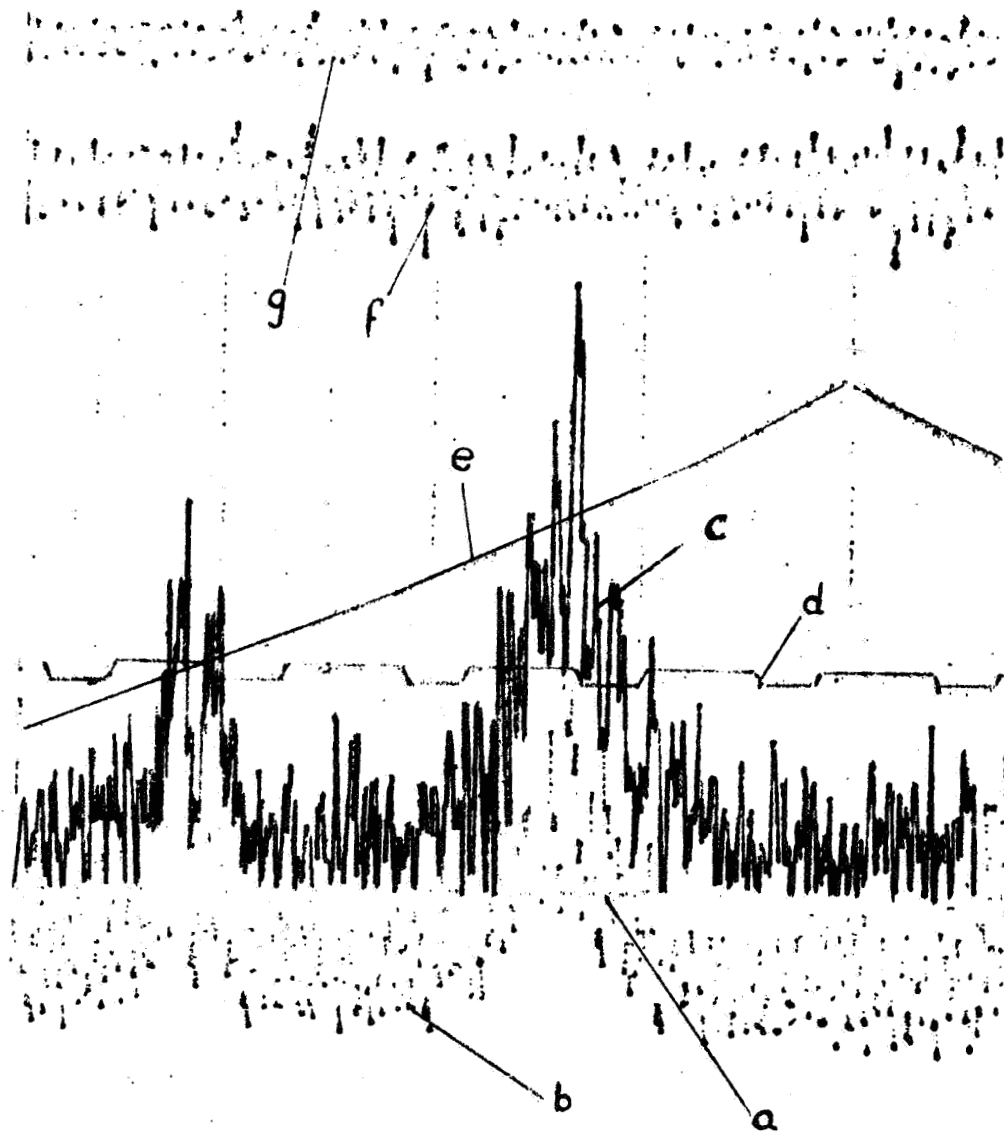


Figure 19 Showing raw data obtained at a scanning rate of 2 scans per second. This record pertains to a region about 1.1 solar radii from the sun's center. Identification of channels is:-

a - spare channel; b - A5303 emission; c - A5303 emission.

Channels b and c record the output of the A5303 amplifier with a ratio of 2:1 in amplitude.

d - corona positional reference channel; e - current through interferometers; f and g - A6374 emission records. (This interferometer failed to operate during eclipse.)

Curves c, d and e have been overwritten to compensate for the poor reproduction quality of the original data paper.

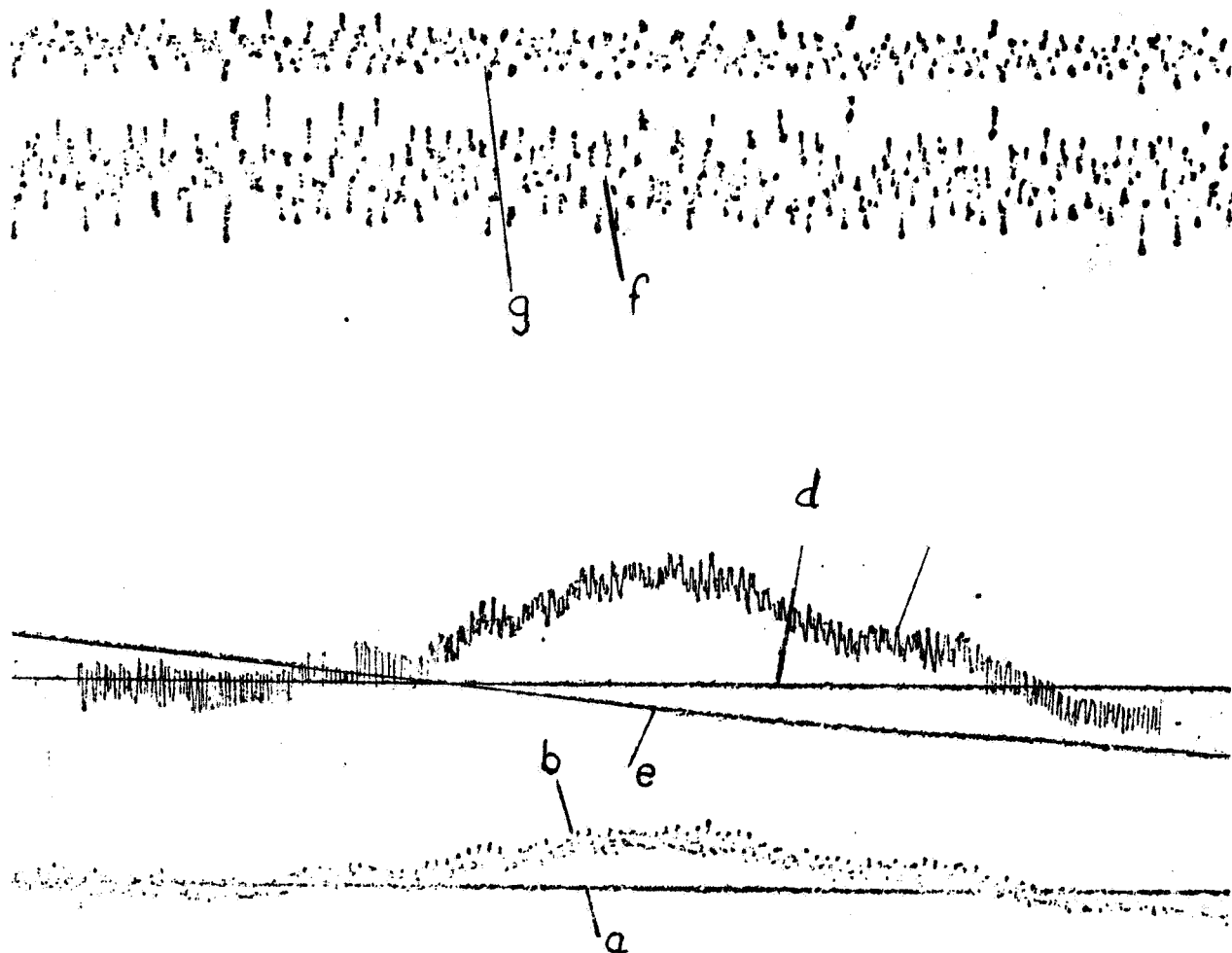


Figure 20 Showing raw data for a scanning rate of about 3 seconds per free spectral range (3.2A). The curves are labeled as in Figure 1. Curves c,d and e have been overwritten to counteract the poor reproduction quality of the original record.

The emission shown on curves b and c corresponds to a region of the corona at 1.6 solar radii from the sun's center at position angle 90°. The profile of c will alter when e, the scanning current, has been linearized.

effective instrumental function which is applied to the observed profiles. A rigorous application of the deconvolution process involves digitizing the various transmission functions and observed profiles. However, due to the amount of noise-in-signal present in the observed profiles, this approach would not be worthwhile. It is considered, from a preliminary survey of the raw data, that a more approximate approach using the "sum of squares" technique, applicable to Gaussian and near-Gaussian profiles, would provide temperature information to an accuracy consistent with the noise-in-signal levels obtained.

A detailed analysis of "halfwidth error" is presented in Appendix B. It is shown there that the fractional error in temperature is given by the following expression (Appendix B, Eq. 20):

$$\frac{dT}{T} \doteq \frac{2M}{C^2 \lambda_o^2} \frac{f^2}{T} \left(\frac{N}{S} \right) \doteq \left(\frac{2}{S} \right) \left(1 + \frac{g^2}{b^2} \right)$$

For the coronal experiment $g \doteq 0.13\overset{o}{\text{\AA}}$ and $b \doteq 1\overset{o}{\text{\AA}}$, therefore,

$$\frac{dT}{T} \doteq \left(\frac{2}{S} \right)$$

Referring to Figure 19, the ratio of the signal to the noise amplitude is about 6:1 for the scan rate of 2 per second. Figure 20 shows the profiles obtained at the much slower rate of one scan per 3 seconds, approximately. Electronic damping improved the signal-to-noise ratio to 16:1. Substituting in the last equation::

$$\frac{S}{N} = 6 \text{ gives } \frac{dT}{T} = 30\%$$

$$\frac{S}{N} = 16 \text{ gives } \frac{dT}{T} = 13\%$$

The essential feature of this observation, which is a novel approach to coronal emission spectroscopy, is to prove the superiority of the photoelectric detection method over that of photography. With longer integration times the accuracy can be increased.

It should be noted that results were obtained in this observation out to $0.8 R_{\odot}$ from the solar limb, where R_{\odot} represents the solar radius. The best previous results at a similar time in the eleven year solar cycle extended to $0.3 R_{\odot}$. These were obtained in 1954 by Jarrett and von Klüber. We therefore have more than doubled the extent of observations of this kind and the technique can undoubtedly be improved in subsequent observations from the experience gained in the eclipse of 1966.

IV. CONCLUSIONS AND SUGGESTIONS FOR FURTHER WORK

The analysis of the data obtained on the $\lambda 5303\overset{o}{\text{\AA}}$ emission will take several months. When completed, about **30** temperatures will be evaluated at various Position Angles out to 1.5 solar radii, and about 15 additional temperatures out to about 1.8 solar radii, near to Position Angle 90° . The performance of this work forms part of a proposal submitted to NASA, Office of Space Science and Applications (IITRI Proposal No. 67-341A). Publication of the final results will be made in late summer of 1967,

One natural follow up of the research performed in this program is the repetition of the observations during other eclipses. Much has been learned from this first attempt and some improvements in the design of the equipment can undoubtedly be found. For example, a change to a reflecting type of telescope with $f/3$ optics and a 10" aperture would provide an increase of about 25 times in the light gathering capability of the system. A simple shock mounting system for the interferometers would greatly reduce the noise contributed by aircraft vibration.

Another follow up to this research is the application of the Scanning Fabry-Perot interferometer to an out-of-eclipse observation of the corona using a coronagraph. Such an application has not to date been attempted although the superior luminosity-resolution product of the Fabry-Perot, coupled with its excellent off-band rejection, indicate that it should

IIT RESEARCH INSTITUTE

provide emission line profile data over a greater extent of the corona than present dispersive techniques can achieve. Noxon⁹ has recently drawn attention to this possibility. This follow up forms a second part of the proposal mentioned above. The proposed program consists of applying the IITRI Scanning Fabry-Perot interferometer, as used in the 1966 eclipse, to the coronagraph situated at the High Altitude Observatory at Climax, Colorado, in the summer of this year. Only slight modification of the equipment in its eclipse form is required in order to adapt it to the 16 inch Climax coronagraph.

ACKNOWLEDGEMENT

I wish to acknowledge the excellent efficiency and constant helpfulness of Dr. Michael Bader and his staff of Ames Research Center during both the preparations and the expedition itself. Completion of the equipment and subsequent conduct of the program would not have been possible without the assistance and interest of many IITRI staff, especially H. Betz, C. Groom (who also flew on the Galileo), and C. W. Terrell,

REFERENCES

1. C. W. Allen, Repts. Prog. Phys., 17, p. 135, 1954.
2. A. Dollfus, C. R., 236, p. 996, 1953.
3. D. E. Billings, Ap. J. 130, p. 961, 1959.
4. A. H. Jarrett and H. von Klüber, M. N., R.A.S., 122, p. 223, 1961.
5. A. Burgess, Ap., J., 139, p. 776, 1964.
6. J. C. Brandt, R. W. Michie and J. P. Cassinelli, Ap. J., 141, p. 809, 1965.
7. W. P. Wright and A. D. Curtis, Sproul Obs. Publ., 11 (no year quoted).
8. A. H. Jarrett and H. von Klüber, M.N., R.A.S., 115, p. 343, 1955.
9. J. Noxon, Ap. J., 145, No. 2, p. 400, 1966.

A P P E N D I X A

A NEW DESIGN OF A SCANNING FABRY-PEROT INTERFEROMETER

A NEW DESIGN OF A SCANNING FABRY-PEROT INTERFEROMETER*

(Short Title: "NEW DESIGN OF SCANNING FABRY-PEROT")

P. N. Slater, H. T. Betz & G. Henderson.

IIT RESEARCH INSTITUTE
Physics Division
Optics Research Section
10 W. 35th Street
Chicago, Illinois 60616

ABSTRACT:

A magnetostrictively scanning Fabry-Perot interferometer is described which has been designed and constructed to be rugged, compact and to require a maximum operating power of 7 watts. Performance tests have shown that it maintains a finesse of about 30 after having been subjected to shock and vibration conditions similar to those encountered during a rocket launch.

The instrument is thus capable of making high resolution measurements from aircraft, balloons, rockets, or space satellites. A satellite experiment to investigate the day airglow and an aircraft or balloon experiment to detect the presence of deuterium on the sun are discussed.

*

Presented at the International Commission for Optics;
Conference on Photographic and Spectroscopic Optics
Tokyo and Kyoto, Japan
September 1 - 8, 1964

INTRODUCTION

Several different methods for changing the order of interference of a Fabry-Perot etalon or interferometer and thereby carrying out a wavelength scan have been described recently in the literature. By far the most commonly described method makes use of a change in density *of* the gas between the etalon plates to change the optical separation of the plates. A number *of* references to this method can be found in the published proceedings(') of the "Colloque International sur les Progrès Récents en Spectroscopie Interférentielle". Mechanical scanning methods have been described by Chabbal and Soulet⁽²⁾, who used a flexible membrane on which was suspended one of the interferometer plates, and by Gobert⁽³⁾ who used a **small** electromagnet to drive one plate against a spring suspension. Roig⁽⁴⁾ changed the separation of the interferometer plates by thermally expanding a bronze cylinder separating the plates. Bradley⁽⁵⁾ used a moving coil vibrator to displace one plate relative to the other. Terhune and Peters⁽⁶⁾ have described a magnetically driven instrument for use in the infrared. Dupeyrat⁽⁷⁾ and Ramsay⁽⁸⁾ have shown that a piezoelectric spacer can be used between the interferometer plates and that, by applying a suitable voltage, the separation can be altered to effect **a** change in the order of interference. Ramsay⁽⁸⁾ has also described a method for maintaining interferometer plate parallelism by means of a servo system which controls the length *of* the piezoelectric spacer

elements. Bennett and Kindlmann⁽⁹⁾ have proposed the use of a magnetostrictive servo control **for** maintaining **a** one meter **long** gaseous laser in tune.

The magnetostrictive servo system proposed by Bennett and Kindlmann⁽⁹⁾ suggested to the present authors the possibility of using **a** magnetostrictive scanning mechanism for a Fabry-Perot interferometer, As such an instrument is photoelectrically recording it can be used for a number of applications in which the photographically recording etalon would be unsuitable. In addition, the scanning interferometer retains the advantages of the etalon over other spectroscopic instruments in its high luminosity and resolving power and its compact size.

INTERFEROMETER DESIGN, CONSTRUCTION, AND **PERFORMANCE**

In Figure 1 is shown the magnetostrictively scanning interferometer developed at IIT Research Institute. For convenience we will refer to the instrument as PRISM (*Photoelectrically Recording Interferometer Scanned Magnetostrictively). The quartz plates of the interferometer are mounted inside a rugged, partially temperature compensated unit constructed of free cut Invar **36**. The temperature compensation is achieved by use of a reentrant design in which only a **6** mm length of Invar is left uncompensated. The total length of the instrument is **12.5** cm and it **is** about 11 cm square in cross section, The separation of the quartz plates is 2.5 mm. The quartz reflecting plates are directly cemented to their Invar support plates with an epcxy resin com-

IIT RESEARCH INSTITUTE

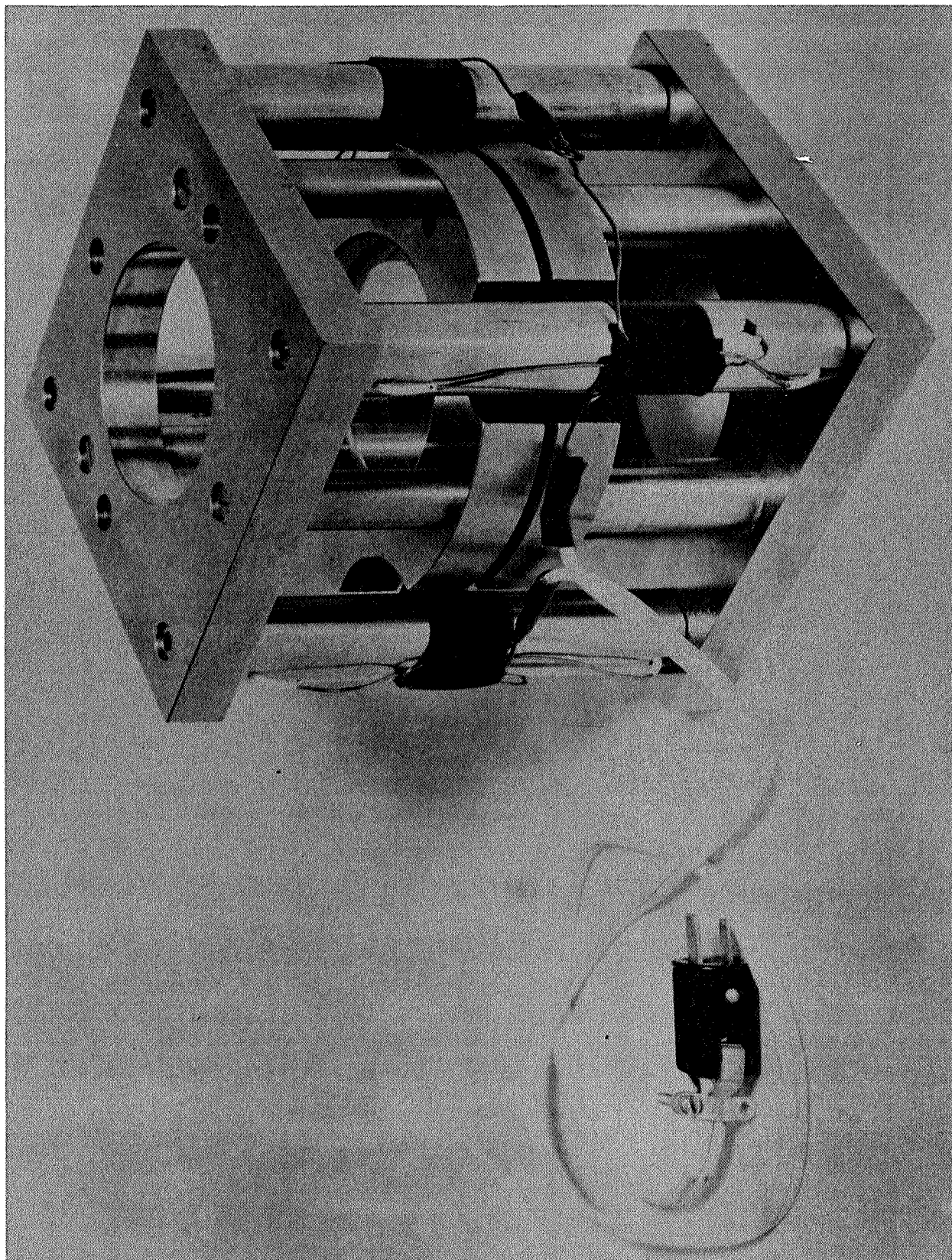


FIG. A1 MAGNETOSTRICTIVELY SCANNED FABRY-PEROT INTERFEROMETER

pound thus eliminating the need for **spring** loaded pressure fingers. This method **of** plate attachment gives the instrument a high degree **of** resistance to misalignment produced by shock and vibration. Parallelism adjustment **is** achieved by careful lapping of the spacer bars, followed by the use of tension bolts through the center of the inner support bars. Each of the four outer support bars shown in Figure 2 consists-of:: (1) an 'Invar rod 3/8" in diameter, (2) 300 turns **of** No, 20 gauge wire wound on an insulating former which fits **loosely** over the Invar rod, (3) an Invar tube, whose annular area **is** the same as the cross sectional area of the Invar rod, in push-fit contact with the end flanges of the inner rod to provide a closed path for the magnetic flux. The four support bar windings are connected in series.

Parenthetically, the first model of **PRISM** that **was** constructed consisted of four solid driver rods with external windings. The end plates in this case **closed** the magnetic field. The support system shown in Figure 2 was constructed to test the closed path magnetic **flux** design, the ultimate aim being to construct a three support or a single tubular support system which would be lighter in weight,.

The rugged construction of **PRISM** makes it suitable for installation in space satellites where it must remain in adjustment beyond the launch phase, Tests carried out on the instrument have **shown** that it remains in adjustment after being **sub-**jected to the loadings listed in Table 1. A second feature of

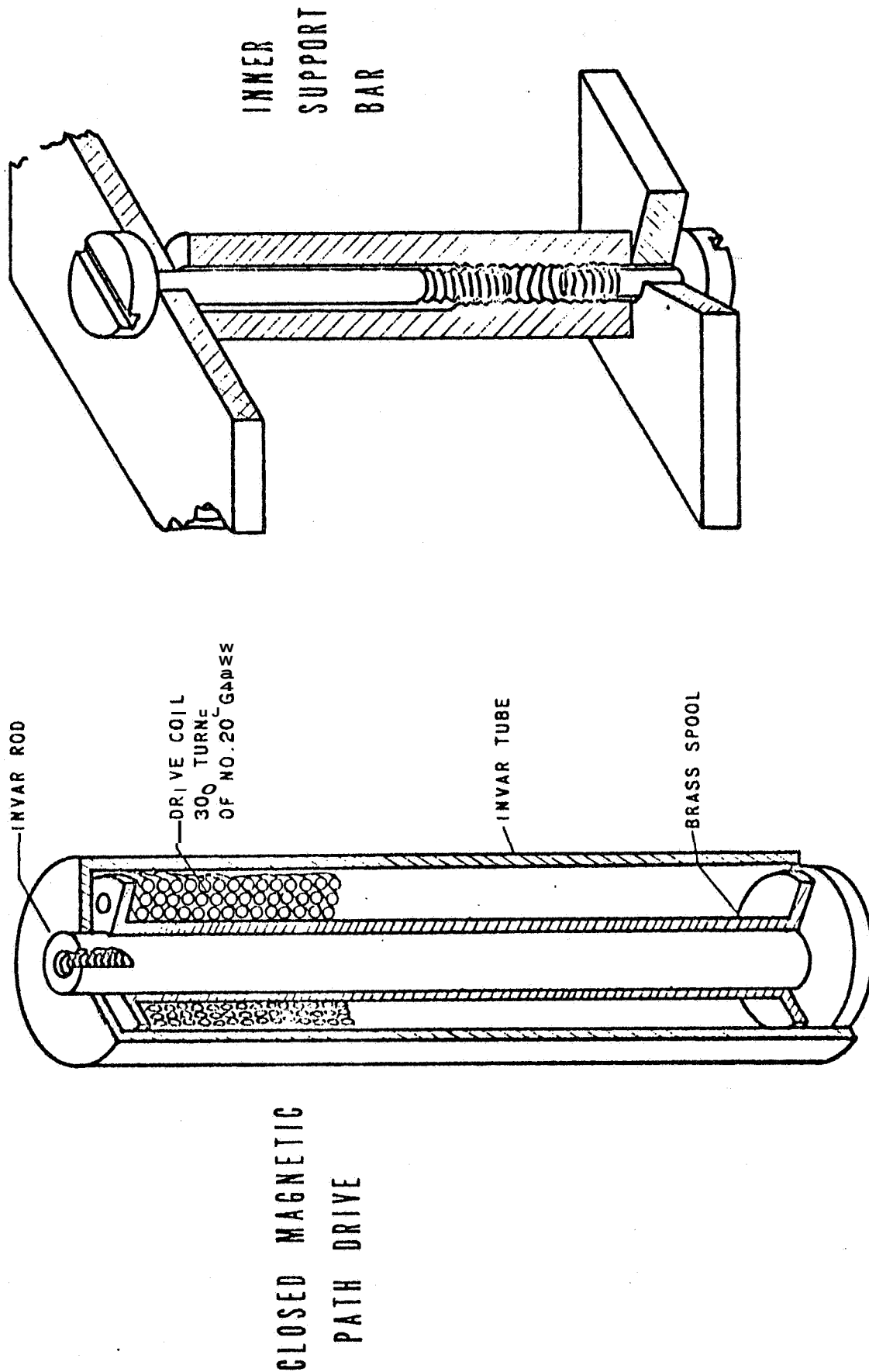
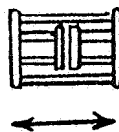


FIG A2 SUPPORT BAR DESIGN

TABLE 1 RESULTS OF VIBRATION TESTS ON INTERFEROMETER

LONGITUDINAL VIBRATION TESTS



<u>Peak "g" Load</u>	<u>No. of Scans</u>	<u>Frequency Range</u>	<u>Scan Rates Octaves/Min</u>
1.5 to 4.5	6	15 to 30 cps	1
1.0 to 8.0	6	25 to 83 cps	4
1.0 to 4.0	6	50 to 2000 cps	4

LAT BAL VIBRATION TESTS



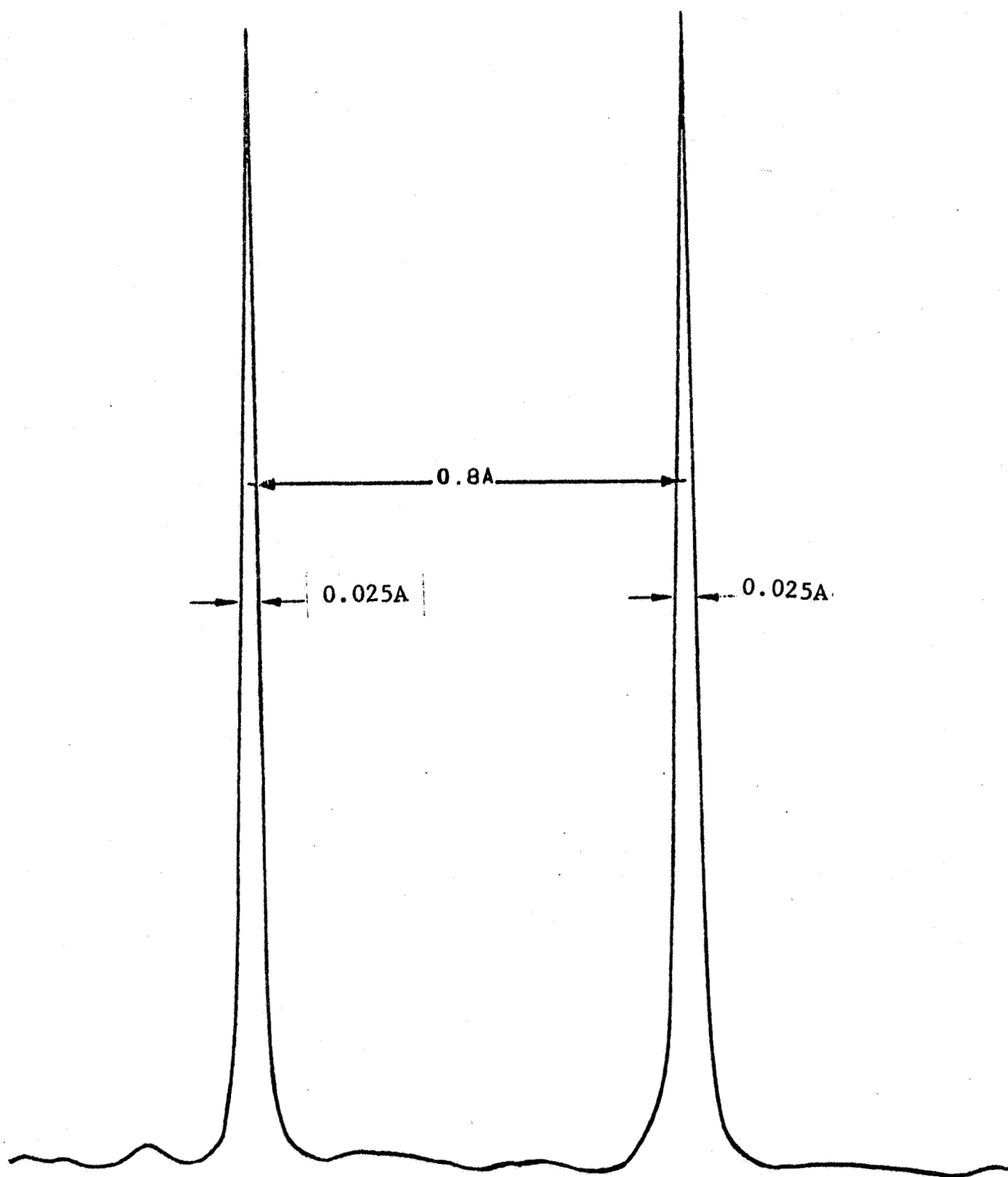
<u>Peak "g" Load</u>	<u>No. of Scans</u>	<u>Frequency Range</u>	<u>Scan Rates Octaves/Min.</u>
1.0 to 4.5	6	15 to 85 cps	4
6.5 to 8.5	6	25 to 87 cps	4
1.0 to 3.0	6	87 to 2000 cps	4

the instrument, which should be mentioned in connection with **its** use as **a** satellite borne instrument, is the low value of **the** magnetic field in the vicinity of the instrument, **At** one meter from the instrument along the optical axis the field strength is 0.1 gamma and at one meter perpendicular **to** the optical axis the field strength is 3.0 gamma, No attempt has been made to reduce these values by the use of magnetic shielding.

The finesse of the interferometer depends on the reflectance and flatness of the quartz plates. The plates used in this work have an approximate reflectance of 96%, transmittance of **3.5%**, and absorptance of 0.5%, and are flat over an area of 18 **sq.** cm. to $\lambda/100$ at $\lambda 6300\text{\AA}$. These values give an effective instrumental width at half height of **0.02A** for a finesse of **40..** Figure **3** shows a trace obtained from a cadmium source at a wavelength of **64388**. The measured half width of the line is **0.025A** for a finesse of 30 which is in reasonable agreement with the calculated value.

The interferometer has been installed in **a** magnesium alloy case which includes simple optics designed to minimize stray light and to focus the ring pattern onto an aperture of angular diameter appropriate **to** the resolving power of the interferometer⁽¹⁰⁾. The unit, shown in Figure **4**, weighs about **25** pounds and occupies a volume of about 1 cu. ft. The maximum power consumption is about 7 watts. The detector, mounted on the **top** of the case, is a 14 stage ruggedized 541E model **EMR** photo-multiplier with an **S20** response, With an applied voltage of

FIG. A3 SCAN OF CADMIUM RED LINE



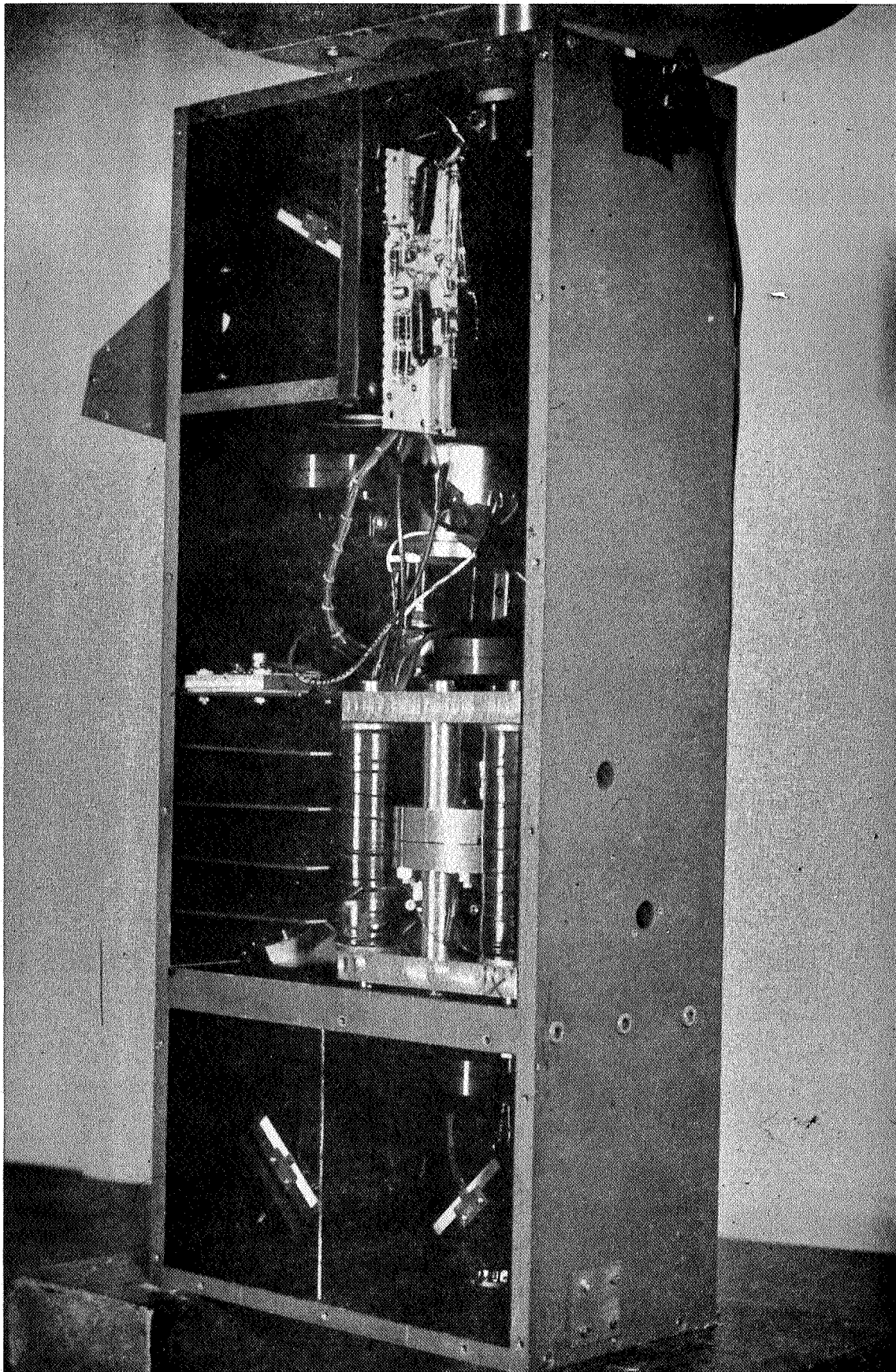


FIG. A4 BALLOON BORNE INTERFEROMETER-SPECTROMETER

2.4 Kv and a gain of 10^6 , the measured dark current and the dark current noise are 5×10^{-12} amps and 6×10^{-12} amps, respectively with the tube cooled to -25°C .

APPLICATIONS OF THE INTERFEROMETER

Two experiments, which make use of the rugged construction of PRISM, will be briefly described here. The first of these is an experiment designed to measure day airglow. We wish to determine the geographical, temporal and seasonal variations of the absolute intensity, and vertical distribution of the $\lambda 6300\text{\AA}$ day airglow which is due to atomic oxygen, and the mean kinetic temperature of oxygen in the emitting region. Using a resolution of about 0.02\AA , we expect to be able to obtain a measure for the Doppler broadened half width of the emission line. Used in an earth satellite of suitable eccentric orbit, e.g. an Orbiting Geophysical Observatory, the instrument will be able to measure the variation of the emission intensity with altitude. Also, the earth's rotation around the sun during the year will provide a measure of the seasonal variation of the emission.

The second experiment is an attempt to detect a deuterium contribution in the H_α Fraunhofer line of the solar spectrum. Various attempts have been made on this problem during the last 12 years or so, notably by Claas⁽¹¹⁾, de Jager⁽¹²⁾, Kinman⁽¹³⁾ and Severny⁽¹⁴⁾. These workers used ground based observations and consequently were hampered by the presence of telluric water

vapor lines in the region of interest of the solar spectrum. By using the scanning Fabry-Perot interferometer installed in a high flying aircraft or balloon, we hope to overcome this difficulty because the total precipitable water vapor along the line of sight is down by 2.5 orders of magnitude at an altitude of 15 Km.

Up to date a lower limit on the D/H ratio has been set by Kinman⁽¹³⁾ at 4×10^{-5} , employing photographic detection. However, the latest theoretical estimate of the D/H ratio in the photosphere is 1×10^{-5} .⁽¹⁵⁾ With a signal to noise ratio of 2:1 the minimum detectable signal variation for the instrument is 0.02% of that due to the continuum in the H_{α} region. This corresponds to a detectability limit for deuterium of 0.04 mÅ equivalent width corresponding to a detectability limit for the D/H ratio of 1.6×10^{-6} .

CONCLUSION

A magnetostrictively scanning Fabry-Perot interferometer has been designed and constructed to be rugged, compact and to require a maximum power input of 7 watts. Performance tests have shown that it maintains a finesse of about 30 after having undergone shock and vibration conditions similar to those encountered during a rocket launch.

The instrument is thus capable of making high resolution measurements from aircraft, balloons, rockets or space satellites. It therefore makes possible the more detailed investigation of

many interesting upper atmosphere and astronomical phenomena which, for various reasons, cannot be satisfactorily investigated from earth.

ACKNOWLEDGEMENTS

The authors wish to thank Dr. L. Reiffel for helpful suggestions and Mr. C. A. Stone for many valuable discussions and continued encouragement.

REFERENCES - APPENDIX

1. J. de Physique et le Radium 49, 1958.
2. R. Chabbal and M. Soulet, *ibid*, p. 274.
3. J. Gobert, *ibid*, p. 278.
4. J. Roig, *ibid*, p. 284.
5. D. J. Bradley, Proc. Roy. Soc. A, 262, 529, 1961.
6. R. W. Terhune and C. W. Peters, J. Opt. Soc. Am., 51, 530, 1961.
7. R. Dupeyrat, J. de Physique et le Radium 19, p. 290, 1958.
8. J. V. Ramsay, Appl. Opt., 1, 411, 1962.
9. W. R. Bennett, Jr., and P. J. Kindlmann, Rev. Sci. Instr., 33, 601, 1962.
10. P. Jacquinot, J. Opt. Soc. Am., 44, 761, 1954.
11. W. J. Claas, Recherches Utrecht, 12, 36, 1951.
12. C. de Jager, Soc. Roy. Sci. Liege, XIV, 460, 1954.
13. T. D. Kinman, M. N. 116, 77, 1956.
14. A. B. Severny, Doklady Akad. Nauk., SSSR, 97, 789, 1954.
15. A. B. Severny, Pub. Crimean Ap. Obs., 16, 12, 1956.
Russian Astr. J., 34, 328, 1957.

APPENDIX B
HALFWIDTH ERROR ANALYSIS

In the determination of temperatures from Doppler-broadened line shapes, it is necessary to first remove the influence of the instrumental function. Rigorously, this is a rather involved procedure using digital computation methods. In many cases, a much simpler approximate method using only the halfwidths of the various functions is quite satisfactory, particularly when the signal-to-noise ratio of the measurement is low. For this reason it is of interest to examine the accuracy of the temperature determination when such a halfwidth method is employed. We start with the basic relation

$$F(\lambda) = B(\lambda) * G(\lambda) \quad (1)$$

$G(\lambda)$ is the instrument function and $*$ denotes convolution

$$F(\lambda) = \int_{-\infty}^{+\infty} B(\lambda') G(\lambda - \lambda') d\lambda' \quad (2)$$

The halfwidths of these functions will be denoted by f , b , g . If B and G are Gaussian profiles then,

$$f^2 = b^2 + g^2 \quad (3)$$

Since $B(\lambda)$ represents a Doppler broadened emission line, it will be Gaussian. On the other hand, the instrument function needs to be examined. If A is the Airy function (representing a perfect Fabry-Perot etalon), E is the function describing the etalon's departure from a perfect etalon and D is the aperture function, then

$$G = A * E * D \quad (4)$$

Empirically, we can determine the form of G by scanning a very narrow emission line. With good Fabry-Perot plates this invariably gives G as a near-Gaussian function.

We are interested in the probable error of the calculated temperature, T , as a function of recording accuracy, signal-to-noise ratio, etc. From $f^2 = b^2 + g^2$ we have

$$b = (f^2 - g^2)^{1/2} \quad (5)$$

The probable error in b is

$$db = \left[\left(\frac{\partial b}{\partial f} df \right)^2 + \left(\frac{\partial b}{\partial g} dg \right)^2 \right]^{1/2} \quad (6)$$

or

$$db = \left[\left(\frac{f}{b} df \right)^2 + \left(\frac{g}{b} dg \right)^2 \right]^{1/2} \quad (7)$$

where df and dg are the probable errors in f and g , respectively.

The fractional probable error in b is then

$$\left(\frac{db}{b} \right) = \frac{f^2 g^2}{b^2} \left[\frac{1}{g^4} \left(\frac{df}{f} \right)^2 + \frac{1}{f^4} \left(\frac{dg}{g} \right)^2 \right]^{1/2} \quad (8)$$

IIT RESEARCH INSTITUTE

The halfwidth of a Doppler broadened line is given by

$$b = C \lambda_o \left(\frac{T}{M} \right)^{1/2} \quad (9)$$

Therefore,

$$\frac{db}{b} = \frac{\frac{1}{2} \frac{C}{(M)^{1/2}} \lambda_o (T)^{-1/2} dt}{\frac{C \lambda_o}{(M)^{1/2}} T^{1/2}} = \frac{1}{2} \frac{dT}{T} \quad (10)$$

Substituting (1) in (8) gives

$$\frac{dT}{T} = \frac{2f^2 g^2}{C^2 \lambda_o^2 \frac{M}{T}} \left[\frac{1}{g^4} \left(\frac{df}{f} \right)^2 + \frac{1}{f^4} \left(\frac{dg}{g} \right)^2 \right]^{1/2} \quad (11)$$

$$\text{i.e., } \frac{dT}{T} = \frac{2M f^2 g^2}{C^2 \lambda_o^2 T} \left[\frac{1}{g^4} \left(\frac{df}{f} \right)^2 + \frac{1}{f^4} \left(\frac{dg}{g} \right)^2 \right]^{1/2} \quad (12)$$

The halfwidth g can be determined through the use of a narrow, well known reference line. Assuming the Fabry-Perot finesse to be the same for both source and reference line we have

$$(f')^2 = g^2 + s^2$$

where f' is the halfwidth of the recorded profile and s is the halfwidth of the reference line.

$$\left(\frac{dg}{g} \right)^2 = \frac{s^4 (f')^4}{g^4} \left[\frac{1}{s^4} \left(\frac{df'}{f'} \right)^2 + \frac{1}{(f')^4} \left(\frac{ds}{s} \right)^2 \right] \quad (13)$$

IIT RESEARCH INSTITUTE

and

$$\frac{dT}{T} = \frac{2M}{C^2 \lambda_0^2} \frac{f^2 g^2}{T} \left[\frac{1}{g^4} \left(\frac{df}{f} \right)^2 + \frac{1}{f^4} \left(\frac{s^4 (f')^4}{g^4} \right) \right. \\ \left. \left\{ \frac{1}{s^4} \left(\frac{df'}{f'} \right)^2 + \frac{1}{(f')^4} \left(\frac{ds}{s} \right)^2 \right\} \right]^{1/2},$$

$$\text{i.e., } \frac{dT}{T} = \frac{2M}{C^2 \lambda_0^2} \frac{f^2}{T} \left[\left(\frac{df}{f} \right)^2 + \left(\frac{f'}{f} \right) \left(\frac{df'}{f'} \right)^2 + \left(\frac{s}{f} \right)^4 \left(\frac{ds}{s} \right)^2 \right]^{1/2} \text{---(14).}$$

The most convenient description of $\frac{df}{f}$ and $\frac{df'}{f'}$ is in terms of the recorded amplitudes I and I' , that is, in terms of $\frac{dI}{I}$ and $\frac{dI'}{I'}$. For Gaussian functions

$$\frac{df}{f} = -0.7 \frac{dI}{I}, \quad \frac{df'}{f'} = -0.7 \frac{dI'}{I'}$$

and

$$\frac{dT}{T} = \frac{2M}{C^2 \lambda_0^2} \frac{f^2}{T} \left[0.5 \left(\frac{dI}{I} \right)^2 + \left(\frac{f'}{f} \right)^4 0.5 \left(\frac{dI'}{I'} \right)^2 \right. \\ \left. + \left(\frac{s}{f} \right)^4 \left(\frac{ds}{s} \right)^2 \right]^{1/2} \text{-----(15)}$$

In terms of the recording accuracy and the signal-to-noise ratio we have

$$\left(\frac{dI}{I} \right)^2 = \left(1.4 \frac{N}{S} \right)^2 + \left(\frac{dx}{x} \right)^2 \text{-----(16)}$$

IIT RESEARCH INSTITUTE

$$\left(\frac{dI'}{I'}\right) = \left(\frac{dx}{x}\right) \quad (17)$$

where $\frac{S}{N}$ = signal-to-noise for the source line, $\frac{dx}{x}$ is the fractional probable error in recording. Then

$$\frac{dT}{T} = \frac{2M}{C^2 \lambda_o^2} \frac{f^2}{T} \left[\frac{1.96}{2} \left(\frac{N}{S}\right)^2 + \frac{1}{2} \left(\frac{dx}{x}\right)^2 + \left(\frac{f'}{f}\right)^4 + \left(\frac{dx}{x}\right)^2 + \left(\frac{s}{f}\right)^4 \left(\frac{ds}{s}\right)^2 \right]^{1/2} \quad (18)$$

$$\frac{dT}{T} = \frac{2M}{C^2 \lambda_o^2} \frac{f^2}{T} \left[\left(\frac{N}{S}\right)^2 + \left[\left(\frac{dx}{x}\right)^2 \frac{1}{2} + \left(\frac{f'}{f}\right)^4 \right] + \left(\frac{s}{f}\right)^4 \left(\frac{ds}{s}\right)^2 \right]^{1/2} \quad (19)$$

As long as s is small compared to f , the signal-to-noise ratio will be the limiting quantity on the temperature accuracy. At low S/N we have

$$\frac{dT}{T} \div \frac{2M}{C^2 \lambda_o^2} \frac{f^2}{T} \left(\frac{N}{S}\right) \div \left(\frac{2}{S/N}\right) \left(1 + \frac{g^2}{b^2}\right) \quad (20)$$

DISTRIBUTION LIST

<u>No. of Copies</u>	Recipient
25	National Aeronautics and Space Administration Office of Research Grants & Contracts, Code BG Washington, D.C. 20546 Attention: Technical Reports Officer
1	IIT Research Institute V. H. Disney
1	IIT Research Institute C. W. Terrell
1	IIT Research Institute J. W. Slade
7	IIT Research Institute Optics Files

IIT RESEARCH INSTITUTE